

TO FLOCK OR NOT TO FLOCK: PROS AND CONS OF FLOCKING IN
LONG-RANGE “MIGRATION” OF MOBILE ROBOT SWARMS

A THESIS SUBMITTED TO
THE GRADUATE SCHOOL OF NATURAL AND APPLIED SCIENCES
OF
MIDDLE EAST TECHNICAL UNIVERSITY

BY

FATİH GÖKÇE

IN PARTIAL FULFILLMENT OF THE REQUIREMENTS
FOR
THE DEGREE OF MASTER OF SCIENCE
IN
COMPUTER ENGINEERING

SEPTEMBER 2008

Approval of the thesis:

**TO FLOCK OR NOT TO FLOCK: PROS AND CONS OF FLOCKING IN
LONG-RANGE “MIGRATION” OF MOBILE ROBOT SWARMS**

submitted by **FATİH GÖKÇE** in partial fulfillment of the requirements for the degree
of
**Master of Science in Computer Engineering Department, Middle East
Technical University** by,

Prof. Dr. Canan Özgen
Dean, Graduate School of **Natural and Applied Sciences**

Prof. Dr. Volkan Atalay
Head of Department, **Computer Engineering**

Asst. Prof. Dr. Erol Şahin
Supervisor, **Computer Engineering Department**

Examining Committee Members:

Prof. Dr. Göktürk Üçoluk
Computer Engineering, METU

Asst. Prof. Dr. Erol Şahin
Computer Engineering, METU

Asst. Prof. Dr. Pınar Şenkul
Computer Engineering, METU

Asst. Prof. Dr. Buğra Koku
Mechanical Engineering, METU

Assoc. Prof. Dr. Veysel Gazi
Electrical and Electronics Engineering, TOBB-ETU

Date: _____

I hereby declare that all information in this document has been obtained and presented in accordance with academic rules and ethical conduct. I also declare that, as required by these rules and conduct, I have fully cited and referenced all material and results that are not original to this work.

Name, Last Name: FATİH GÖKÇE

Signature :

ABSTRACT

TO FLOCK OR NOT TO FLOCK: PROS AND CONS OF FLOCKING IN LONG-RANGE “MIGRATION” OF MOBILE ROBOT SWARMS

Gökçe, Fatih

M.S., Department of Computer Engineering

Supervisor : Asst. Prof. Dr. Erol Şahin

September 2008, 46 pages

Every year, certain animal and insect species flock together to make long-range migrations to reach their feeding or breeding grounds. A number of interesting observations can be made regarding this phenomenon. First, individuals tend to create large flocks, which can include millions of individuals in fishes, for these migrations. Second, migrations typically cover long distances. Third, despite all kinds of disturbances affecting the individuals during these migrations, the flocks can reach the very same breeding or feeding grounds with remarkable accuracy. Biological studies indicated that these animals mainly use the magnetic field of earth (among many other environmental cues) to determine the direction of their travel. It was also claimed that migrating in flocks has been the key factor behind the accuracy of reaching the same grounds at the end of the migration.

In this thesis, we take a constructivist approach towards investigating the effects of flocking in long-range travels using a swarm of physical and simulated mobile robots. Specifically, we extend a self-organized flocking behavior that was developed by Turgut et al. (2008) that allows the long-range migration of a robotic swarm in space using the magnetic field of the earth. Using this behavior, we analyze how the accuracy of the robotic swarm reaching a particular “breeding ground” is affected by four factors;

namely, (1) averaging through the heading alignment, (2) noise in sensing the homing direction, (3) differences in the characteristics of the individuals, and (4) disturbances caused by the proximal interactions of the robots during flocking. Through systematic experiments with physical and simulated robots, we analyze how these factors affect the accuracy along with the flock size and different sources of noise.

Keywords: swarm robotics, flocking, migration

ÖZ

SÜRÜ HALİNDE HAREKET ETMEK YA DA ETMEMEK: SÜRÜ HALİNDE HAREKET ETMENİN GEZER ROBOT SÜRÜLERİNİN UZUN MESAFE “GÖÇ” ETMESİNDEKİ AVANTAJ VE DEZAVANTAJLARI

Gökçe, Fatih

Yüksek Lisans, Bilgisayar Mühendisliği Bölümü

Tez Yöneticisi : Yrd. Doç. Dr. Erol Şahin

Eylül 2008, 46 sayfa

Her yıl belirli hayvan ve böcek türleri beslenme veya üreme alanlarına ulaşmak için, uzun mesafeler katederek sürü halinde göç ederler. Bu olgu üzerinde çeşitli gözlemler yapılabilir. Birincisi, bireyler kalabalık sürüler oluşturarak göç etme eğilimindedirler; örneğin balıkların oluşturduğu sürüler, milyonlarca bireyi içerebilir. İkincisi, göçler sırasında çok uzun mesafeler katedilir. Üçüncüsü, bireyleri bu göçler sırasında etkileyebilecek her türlü olumsuz etmene rağmen sürüler, aynı beslenme veya üreme alanlarına çok yüksek bir hassasiyetle ulaşırlar. Biyolojik çalışmalar bu hayvanların yön bulmada genellikle yerin manyetik alanını kullandıklarını göstermektedir (Güneş, yıldızlar, koku gibi diğer birçok mekanizma da kullanılabilir). Ayrıca, elde edilen hassasiyetin arkasındaki temel faktörün, göçlerin sürü halinde yapılması olduğu da öne sürülmüştür.

Bu tezde, yapıcı bir yaklaşımla, sürü halinde hareket etmenin uzun mesafe yolculuklarındaki etkisini, hem fiziksel robotlarla hem de benzetim ortamında inceledik. Özel olarak, Turgut ve arkadaşları (2008) tarafından geliştirilen kendi kendine sürü halinde hareket etme davranışını, bir robot sürüsünü yerin manyetik alanını kullanarak uzun mesafe göç ettirecek şekilde genişlettik. Bu davranışı kullanarak, robot sürüsünün belirli bir üreme alanına ulaşmadaki hassasiyetinin şu dört faktörden nasıl etkilendiğini

analiz ettik: (1) yön ayarlama davranışı ile ortalama alınması, (2) hedef yönü belirlemedeki gürültü, (3) robotlar arasındaki karakteristik farklılıklar, (4) yakınlık kontrolünün yarattığı bozucu etkiler. Fiziksel robotlarla ve benzetim ortamında yaptığımız deneylerle, bu faktörlerin sürünün büyüklüğüne ve çeşitli gürültü kaynaklarının varlığına bağlı olarak hassasiyeti nasıl etkilediğini inceledik.

Anahtar Kelimeler: oğul robot bilimi, sürü halinde hareket etme davranışı, göç

ACKNOWLEDGMENTS

In the first place, I would like to express my sincere gratitude to my advisor, Erol Şahin for his never-ending supervision, advice, and guidance at all levels of the study. The work presented in this thesis would not be possible without him. Thanks for creating such a nice laboratory and for giving me the chance to work with you.

I would like to thank to Andrew M. Simons for his support in obtaining very important papers, encouragement and advice. I am also grateful to Jorgen Rabøl for sending me his paper.

My special thanks go to two very special people: Ali Emre Turgut not only for his endless “helps” whenever and whatever I need beginning from the day we met, but also for his friendship opening a new era in my life. You are the only person in my life having a heart as pure as the music of Erkan Oğur. Hande Çelikkanat for being a perfect companion in every study we worked together, for her generous support on any matter and at any time, for her true friendship and golden heart.

I must thank Emre Uğur for his never-ending encouragement and for always being a positive source of energy.

I am deeply thankful to all Kovan Research Lab. members, Levent Bayındır, Maya Çakmak, Mehmet Remzi Doğar, Onur Soysal, Erkin Bahçeci, Barış Akgün, İlkay Atıl, Nilgün Dağ, Tahir Bilal for creating such a nice atmosphere. I am very lucky to work with you.

I am very thankful to Mehmet Durna, Yaman Çakmakçı, Serkan Güroğlu and Kutluk Bilge Arıkan for their encouragement, support and friendship.

Murat Tamer, my brother and forever friend. Not much to say about you, thanks for everything. I am looking forward to the day we will continue our never-ending discussions.

Special thanks go to Gönenç Ülker a young brilliant scientist and even most importantly an art enthusiast. You are my brother and forever friend. I know that I missed the most important times being very busy with my thesis. Sorry about that and thank you for your patience.

My gratitude thanks go to my lovely friends Ali Gök, Ali Sinan Dike, Engin Kursun, Erkan Dođan, Evren Cabi, Ferhat Erdal, Hakan Bayrak, İsmail Yıldız, Mehmet Sorgun, Melih Onay, Serdar Çarbaş and Serdar Karakurt. You are my family in METU.

I believe that there is nothing enough to express my thanks to you, my mother, father and sister, but a success that will forget you the hard times. This study is dedicated to that purpose. I am nothing without you.

I know that the list will expand as I write. But there should be an end. I want to end up by thanking all people that I could not mention here.

The experiments with physical robots in this study are conducted in the hall at the deanery building of Faculty of Arts and Sciences at Middle East Technical University. I would like to express my gratitude to all staff in the dean’s office and especially to Gönül Urgan, Secretary of Faculty of Arts and Sciences, for giving us the opportunity to use the hall and for her encouragement.

The simulations in this study are conducted on the High Performance Computing Center of the Department of Computer Engineering at Middle East Technical University. I would like to thank all people involved and especially to Çelebi Kocair for his great support in finding solutions to all my requests.

Being currently enrolled in Faculty Development Program(ÖYP) in Middle East Technical University on behalf of Süleyman Demirel University, I am indebted to thank all people involved in Faculty Development Program.

This study is mainly funded by The Scientific and Technological Research Council of Turkey (TÜBİTAK) through the “KARİYER: Kontrol Edilebilir Robot Ođulları” project with number 104E066.

To my family

TABLE OF CONTENTS

ABSTRACT	iv
ÖZ	vi
ACKNOWLEDGMENTS	viii
DEDICATON	x
TABLE OF CONTENTS	xi
LIST OF FIGURES	xiii
LIST OF TABLES	xvi
CHAPTERS	
1 INTRODUCTION	1
2 RELATED WORK	4
2.1 Thesis Problem	7
3 EXPERIMENTAL PLATFORMS	8
3.1 The Kobot Robot Platform	8
3.1.1 The Infrared Short-range Sensing Sub-system	8
3.1.2 The Heading Sensing Sub-system	14
3.2 The Simulator: Co-Swarm	15
4 THE FLOCKING BEHAVIOR	16
4.1 Heading Alignment Behavior	16
4.2 Proximal Control Behavior	16
4.3 Homing Behavior	17
4.4 Motion Control	19
5 EXPERIMENTAL FRAMEWORK	20
5.1 Setup	20
5.1.1 Kobots	21
5.1.2 CoSS	22
5.2 Metrics	23
5.2.1 Inter-quartile and Whisker Ranges	23

	5.2.2	Average Speed	25
6		FACTORS THAT INFLUENCE LONG-RANGE MIGRATION OF FLOCKS	26
7		EXPERIMENTS	29
	7.1	Effect of Proximal Disturbance	30
	7.2	Effect of Noise in Sensing the Homing Direction	31
	7.3	Effect of Proximal Disturbance with Noise in Sensing the Hom- ing Direction	33
	7.4	Effect of Individual Differences with Noise in Sensing the Hom- ing Direction	35
	7.4.1	Without Proximal Control	37
	7.4.2	With Proximal Control	38
		7.4.2.1 CoSS Experiments	38
		7.4.2.2 Kobot Experiments	38
8		CONCLUSION	43
		REFERENCES	45

LIST OF FIGURES

FIGURES

<p>Figure 3.1 (a) Photo of a Kobot. (b) The scaled drawing of Kobot illustrating the circular body, wheels, placement of the sensors and range for 2^{nd} sensor. The sensors are placed uniformly at 45° intervals. Each square patch in the gray scale blob indicates the output of the sensor averaged over 200 samples. A white plastic stick with a diameter of 2 cm is used as the target. Darker colors denote higher values of sensor measurement. (Images are taken from [1].)</p>	9
<p>Figure 3.2 Block Diagram of Kobot. (Image is taken from [2].)</p>	9
<p>Figure 3.3 (a) Photo of a sensor board. (b) Block diagram of an individual sensor. (Images are taken from [2].)</p>	10
<p>Figure 3.4 Timing diagram of a sensor detecting an obstacle. (Image is taken from [2].)</p>	12
<p>Figure 3.5 The order and timing of sensors put into the <i>proximity-sensing</i> state by the main sensor controller. First, even numbered sensors and after 2 ms, odd numbered sensors are put into the <i>proximity-sensing</i> state.</p>	12
<p>Figure 4.1 Plot of the virtual force with respect to o_k. o_{des} is set to 3 for kin-robots. The value of o_k increases as the distance gets closer. The virtual force always takes values within $[-1, 1]$ interval. (Image is taken from [2].)</p>	17

Figure 4.2	The body-fixed reference frame of Kobot is depicted. It is fixed to the center of the robot. The x -axis of the body-fixed reference frame coincides with the rotation axis of the wheels. The forward velocity (u) is along with the y -axis of the body-fixed reference frame. The angular velocity of the robot is denoted with ω . v_R and v_L are the velocities of the right and left motors, respectively. θ , current heading of the robot, is the angle between the y -axis of the body-fixed reference frame and the <i>sensed North</i> direction (n_s). l is the distance between the wheels. (Image is taken from [2].)	18
Figure 5.1	The topology of the robots for different flock sizes. The arrow indicates the homing direction.	21
Figure 5.2	(a) An overhead view of the experiment arena. (b) The magnetic field measured in the experiment arena. The field is tilted to the left approximately 6-degrees. The units of the axes are in meters.	22
Figure 5.3	(a) The path followed by the center of a single robot. (b) The magnetic field model in the simulations. The units of the axes are in meters.	23
Figure 5.4	(a) In an ideal world, the robots migrate with perfect accuracy. The units of the axes [in (a) and (b)] are in meters. (b) The paths followed by the center of a flock in an environment with noise are drawn for illustrative purposes. (c) Distributions of the center positions, the boxplot of distribution and IQR and WR are illustrated.	24
Figure 6.1	Histogram of simulated noisy sensing the homing direction.	27
Figure 7.1	With no noise in sensing or actuation the flock of any number of robot always follows the same path. The units of the axes are in meters.	29
Figure 7.2	(a) Plot of IQR & WR for different flock sizes while the only noise source is proximal control. (b) Plot of average speed for different flock sizes. The horizontal axis is in log scale. The dashed line indicates the value of the maximum forward speed $u_{max} = 0.07$ m/s.	31
Figure 7.3	The paths followed by the flocks for $\eta_S = 0.5$. The units of the axes are in meters. $[0,0]$ is the starting point. (a) 1 robot, (b) 3 robots, (c) 7 robots, (d) 19 robots, (e) 91 robots.	32

Figure 7.4	Effect of η_S . Plot of IQR with respect to η_S for different flock sizes.	33
Figure 7.5	Plot of IQR & WR for different flock sizes while (a) $\eta_S = 0.1$, (b) $\eta_S = 0.9$.	33
Figure 7.6	(a) Plot of V_a with respect to flock size for different values of η_S . Horizontal axis is in log scale. (b) Plot of V_a with respect to η_S for different flock sizes. The dashed lines indicate the value of the maximum forward speed $u_{max} = 0.07$ m/s.	34
Figure 7.7	Plot of IQR with respect to η_S for different flock sizes.	35
Figure 7.8	Plot of IQR & WR in proximal disturbance experiments for different flock sizes while (a) $\eta_S = 0.1$, (b) $\eta_S = 0.9$.	36
Figure 7.9	(a) Plot of V_a with respect to flock size in proximal disturbance ex- periments for different values of η_S . Horizontal axis is in log scale. (b) Plot of V_a with respect to η_S for different flock sizes. The dashed lines indicate the value of the maximum forward speed $u_{max} = 0.07$ m/s.	36
Figure 7.10	Characteristics of different robots after adding actuation noise. (a) Box- plot of deviations, (b) IQR & WR plots.	37
Figure 7.11	IQR & WR plots for individual difference experiments while the proximal control is disabled and enabled.	38
Figure 7.12	Actuation characteristics of Kobots at 2 m while moving forward.	39
Figure 7.13	The individual differences between Kobots. (a) Distribution of de- viations at final position are given. Note that due to a 6-degrees deviation to the one side of the corridor, deviation values are mostly negative. (b) IQR and WR plots calculated from the boxplots in (a).	40
Figure 7.14	The selection and initial placement of the flocks are given for Kobot experiments.	41
Figure 7.15	IQR and WR of joint distributions of single robot experiments and two 5-Kobot flocks and 7-Kobot flock.	42

LIST OF TABLES

TABLES

Table 5.1	The default parameter settings for the behavior.	21
Table 7.1	Investigated factors in the experiments. The four factors considered are HA: Averaging through heading alignment, HD: Noise in sensing the homing direction, CD: Differences in the characteristics of the individuals and PD: Disturbances caused by proximal control behavior.	30
Table 7.2	The number of the groups selected from 91 diversified robots randomly.	37

CHAPTER 1

INTRODUCTION

In the near future, advances in technology is likely to enable the mass production of robots. The availability of swarms of relatively simple and cheap robots would allow us to take an alternative approach to real-world problems, such as the surveillance of large regions or the de-mining of mine fields. However, tackling such problems require the development of robust and scalable coordination algorithms.

Swarm robotics, is an approach that aims to develop robust, scalable and flexible coordination algorithms for robots using inspiration from nature. In this approach, a complex task, which is beyond the capability of a single individual, is performed by a swarm of robots with only local interactions among the individuals and between the individuals and environment [3].

As inspiration sources, one needs to take look at the amazing coordination strategies that are observed in social insects and animals. Ants build and maintain a colony through which they can successfully forage preys from large regions. Termites can build large mounds from earth. Bird flocks can make long-range migration flights that not only warn off their predators but also allow them to take precise paths to their breeding or feeding grounds.

Swarm robotics works at the intersection of science and engineering. On one hand, it provides a constructive approach to test the hypothesis that has been developed in biological studies on the observed coordination taking place among organisms. On the other, it aims to develop coordination algorithms that can be used to control swarm robotic systems in real-world problems.

In real-world problems, one particular example of coordination problems arises when a swarm of robots needs to travel from an initial point to an operation range. Let's assume that we have a swarm of robots that are assigned to carry out a certain

mission in a distant operation area. Other than the coordination problem in the operation area, we have another crucial problem which is the long-range migration of the swarm of robots to and from the operation area. In such a task, the expectation is that the swarm of robots should reach to the operation range with a high accuracy. One approach to this problem could be to improve the robots individually, so that each of them follows an accurate path and arrives the operation area in an accurate manner. This approach will require development of complex algorithms and even improvement of hardware components. But what if to use the swarm robotics approach and to exploit being together in a swarm?

As inspiration source, we have a widely observed phenomenon in nature, long-range migration. Every year, certain animal and insect species flock together to make long-range migrations to reach their feeding or breeding grounds. A number of interesting observations can be made regarding this phenomenon. First, individuals tend to create large flocks, which can include millions of individuals in fishes, for these migrations. Second, migrations typically cover long distances. Third, despite all kinds of disturbances affecting the individuals during these migrations, the flocks can reach the very same breeding or feeding grounds with remarkable accuracy. Biological studies indicated that these animals mainly use the magnetic field of earth (among many other environmental cues) to determine the direction of their travel. It was also claimed that migrating in flocks has been the key factor behind the accuracy of reaching the same grounds at the end of the migration.

In this thesis, we take a constructivist approach towards investigating the effects of flocking in long-range travels using a swarm of physical and simulated mobile robots. Specifically, we extend a self-organized flocking behavior that was developed by Turgut et al. [1] that allows the long-range migration of a robotic swarm in space using the magnetic field of the earth. Using this behavior, we analyze how the accuracy of the robotic swarm reaching a particular “breeding ground” is affected by four factors; namely, (1) averaging through the heading alignment, (2) noise in sensing the homing direction, (3) differences in the characteristics of the individuals, and (4) disturbances caused by the proximal interactions of the robots during flocking. Conducting systematic experiments with physical and simulated robots, we analyze how these factors affect the accuracy along with the flock size and different sources of noise.

The rest of the thesis is organized as follows. In the next chapter, we review

the related work in biology and robotics. In Chapter 3, we describe the robotic platform and the simulator we used. Then, the flocking behavior is presented in Chapter 4. Chapter 5 presents the setups used in the experiments and the metrics utilized. In Chapter 6, the factors that influence the accuracy of the flocking behavior are introduced and described. The experiments and their results are presented in Chapter 7. The conclusions are provided in Chapter 8.

CHAPTER 2

RELATED WORK

“The story of migrating birds is the story of a promise: The promise to return.”

— from Winged Migration movie [4]

Each year certain insect and animal species make long travels to reach their feeding or breeding places which is called as migration. Migration is an impressive phenomenon because of its three important properties: (1) Very long distances scaling up to several thousands of kilometers are travelled during migration. (2) Migratory animals and insects typically migrate in flocks rather than as individuals. These flocks involve individuals up to several millions. (3) Migration occurs in an accurate way despite the effect of different environmental conditions and hazards.

Arctic terns migrate from Arctic to Antarctic and back making a round-trip journey nearly 35400 km each year. The flocks formed during the migration include large number of individuals. During their migration they utilize a variety of sensing abilities for orientation and navigation. Some birds are shown to use sun compasses. They are also shown to sense [5, 6, 7] and even see [8] the magnetic field of the earth. Some visual landmarks and olfactory cues are also shown to be used in navigation.

Migratory behavior is also observed in fish species, such as sardines. They migrate from east coasts of South Africa to north creating shoals often 7 km long, 1.5 km wide and 30 meters deep. There are some hypothesis for fishes to use magnetic field of the earth like birds and also oceanic electric fields [9].

Among the insects, the monarch butterflies migrate from southern Canada to central Mexico every year where they spend the winter after traversing a distance nearly 3200 km. These insect are shown to use a combination of circadian rhythm and the position of the sun in the sky for navigation [10].

The precision obtained by animals during the migration has attracted many researchers to find an answer to this captivating phenomenon. Although researchers have been working on the navigational mechanisms utilized by individuals and increasing our knowledge on the abilities of the individuals, the underlying value of flocking behavior in the navigational accuracy is still remains an open question. It was Bergman and Donner [11] first suggesting that the flock migration “increases the accuracy of orientation mechanism” which is known as the *many wrongs principle*. They suggested that flocking suppresses the tendencies of the individuals to migrate in slightly different directions, hence the flock can align to an average direction of the preferences of the individuals giving a more accurate direction when compared to the case of individual birds.

Hamilton [12] and Wallraff [13] reiterated the *many wrongs principle* in their theoretical studies. Hamilton suggested that “the orientation of groups of animals is more accurate than that of individuals”. Assuming that (1) spatial goal is same for all individuals, (2) inaccuracies are represented by the deviation of the individuals from the goal and (3) individuals adopt their orientation to the mean direction of the individuals in the flock, he drew a series of theoretical curves with respect to flock size showing that average deviation from goal decreases with the flock size. Wallraff suggested some methods to analyze the observational data to investigate the effect of flocking to the accuracy of orientation toward the goal direction and described their statistical implications.

In [14], Rabøl et al. observed skylark flocks of different sizes (1,2, 3-5, and 6 or more) on their spring migration. They showed that the dispersion of the migratory directions becomes less scattered with the size of the flock. Later, Tamm [15] observed similar results testing the hypothesis on homing pigeons with three to six flocks. By selecting flocks in a random fashion, he obtained that the flocks are more accurate than individuals and their homing time is shorter than that of singles.

Besides the promising field observations, some contradictory observations are also reported. In [16], Keeton compared mean bearings of single pigeons with that of flocks of four pigeons. He reported no significant difference between single birds and flocks in terms of accuracy. In [17], Benvenuti et al. performed experiments to compare orientation behavior of single birds with that of small flocks including three and ten birds. Their results showed that small flocks do not orient more accurately than

single birds. In [18], Guilford et al. performed experiments by releasing pairs of homing pigeons in which none, one or both of the birds had previously been trained. They investigated whether unexperienced birds exploit the knowledge of other bird to achieve a navigational advantage or not. They found that unexperienced birds do not prefer to home together with their pairs, be it experienced or not.

Recently, Simons has brought the almost forgotten *many wrongs principle* to light as a null model and general framework for testing the advantage of group navigation empirically [19]. Taking the *many wrongs principle* in its simplest form in which there are no characteristic differences between individuals and contribution of individuals to the direction of flock are equal, he showed that large group size increases the accuracy of group navigation. He emphasized that the principle can be generalized to more complex scenarios in which there are differences between individuals and the individuals contribute to flock direction in an unequal manner.

The work of Simons has attracted some attention to the *many wrongs principle*. In [20], Hancock et al. developed a model to investigate the navigational foraging advantages of aggregation behavior in nomadic animals in particular bearded pigs. They modeled the movement and aggregation strategies of individuals with two parameters. The first parameter controls the food sensing ability of an individual, whereas the second one controls the tendency of an individual to aggregate or avoid its neighbors. The latter parameter is evolved via a genetic algorithm. Their results show that the evolved parameter indicate optimality of aggregation if two conditions both hold: (1) the environment has high quality but rare food sources, (2) the use of decision of other group members is sufficient due to the uncertainty in the sensing power of an individual. The optimality of aggregation under these two conditions demonstrate the *many wrongs principle*.

In another study, Codling et al. studied the *many wrongs principle* in a scenario resembling to the migration of animals [21]. They developed a point-mass movement model incorporating a biased random walk behavior and the group interactions. They investigated the effect of navigational error, group size, interaction radius size and environmental turbulence to the performance of the behavior to navigate a group from one location to another. They find that, other than the high environmental turbulence case, the group movement has a navigational advantage.

A related problem was also studied in robotics. Gutierrez et al. proposed a fully-

distributed strategy for the improvement of odometry in collective robotics [22]. In this strategy, the robots improve their estimate of location by exploiting the estimations of their neighbors. The estimate of each robot is associated with a confidence level decreasing with the distance travelled by the corresponding robot. Each robot combines its own estimate and the received estimates of its neighbors using the confidence level of each estimate to get a more precise location information. Authors evaluated their strategy in simulations on a foraging task in which the duty of the robots is to bring items from a resource site to a central place. They found that as the group size is increased both the quality of the individuals' estimates and the performance of the group are improved.

Although the interest in the role of flocking in long-range migrations, as reviewed above, have produced a number of hypotheses and models in biological systems, many questions remain unanswered. Despite the results obtained in simulations, coupled with few, sometimes contradictory observational data from animal flocks, the problem begs a constructivist approach.

2.1 Thesis Problem

In this thesis, we are interested in how flocking affects the accuracy of long-range migration in a swarm of individuals. Inspired by the biological studies reviewed above, we are interested in developing a flocking behavior for a swarm of robots that use the magnetic field of the earth to emulate a simple form of long-range migration in space. Through a systematic set of experiments conducted using physical robots as well as physics-based realistic robot simulations, we aim to analyze pros and cons of flocking in the long-range "migration" of mobile robot swarms and to expand our understanding of this interesting phenomenon in an artificial system to shed light on the biological studies.

CHAPTER 3

EXPERIMENTAL PLATFORMS

In this study, we used Kobot, a mobile robot platform developed as a testbed for swarm robotic research (See Figure 3.1(a)) and its simulator.

3.1 The Kobot Robot Platform

Kobot is a CD-sized, differentially driven and power efficient platform weighing only 350 gr with batteries. Figure 3.2 shows the block diagram of Kobot. It has 8 infrared (IR) sensors capable of kin and obstacle detection and a digital compass. The communication among robots as well as between the robots and a console is carried out through an IEEE 802.15.4/ZigBee compliant wireless communication module with a range of approximately 20 m indoors. The main processor of robot is a 20 MHz *PIC184620A* microcontroller. Thanks to low-power design of the robot, Kobot has an autonomy of 10 hours reported with a 2000 mAh lithium-polymer battery.

In the following two subsections, we give the details of the short-range sensing and the heading sensing sub-systems because of their importance in the behavior we have developed. For the details of other sub-systems please refer to [2].

3.1.1 The Infrared Short-range Sensing Sub-system

The infrared short-range sensing sub-system (IRSS) measures the range and bearing of kin-robots and other objects in close proximity. It consists of eight IR sensors placed uniformly at 45° intervals, as shown in 3.1(b) and 3.3(a) and a main sensor controller. Each sensor is capable of measuring distances up to 20 cm at seven discrete levels and distinguishing robots from obstacles/walls at a rate of 18 Hz. The IR signals utilized in the measurement is modulated at 38 kHz to eliminate environmental noise.

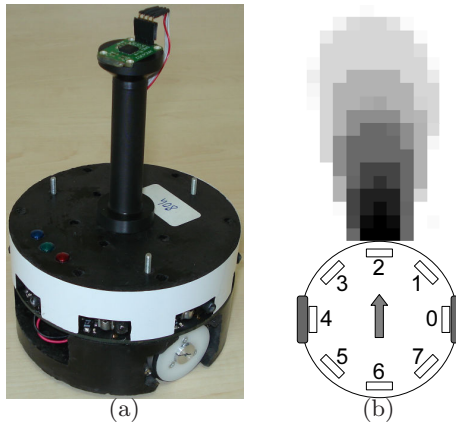


Figure 3.1: (a) Photo of a Kobot. (b) The scaled drawing of Kobot illustrating the circular body, wheels, placement of the sensors and range for 2nd sensor. The sensors are placed uniformly at 45° intervals. Each square patch in the gray scale blob indicates the output of the sensor averaged over 200 samples. A white plastic stick with a diameter of 2 cm is used as the target. Darker colors denote higher values of sensor measurement. (Images are taken from [1].)

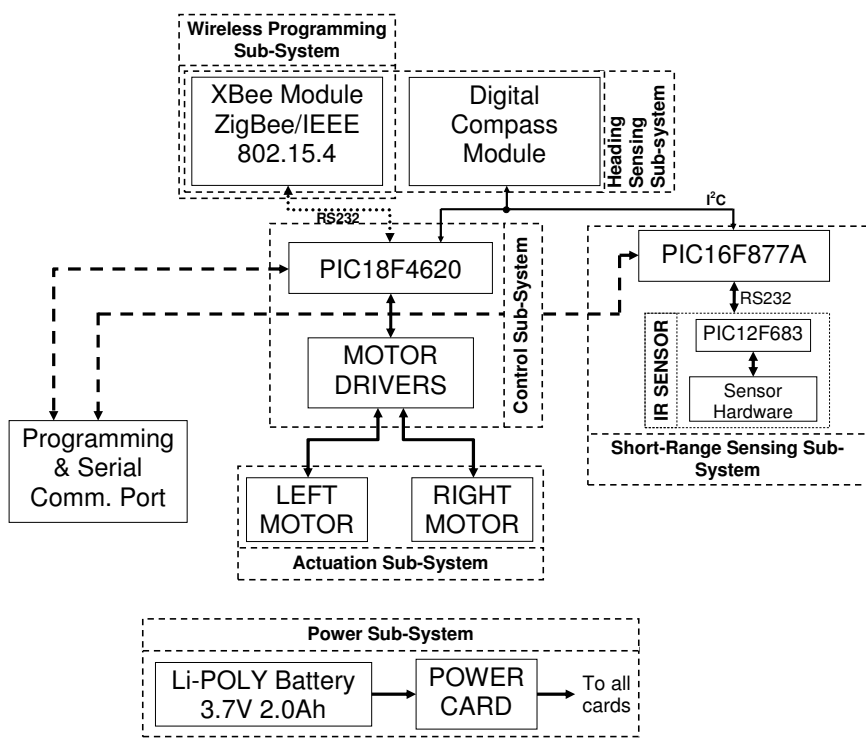


Figure 3.2: Block Diagram of Kobot. (Image is taken from [2].)

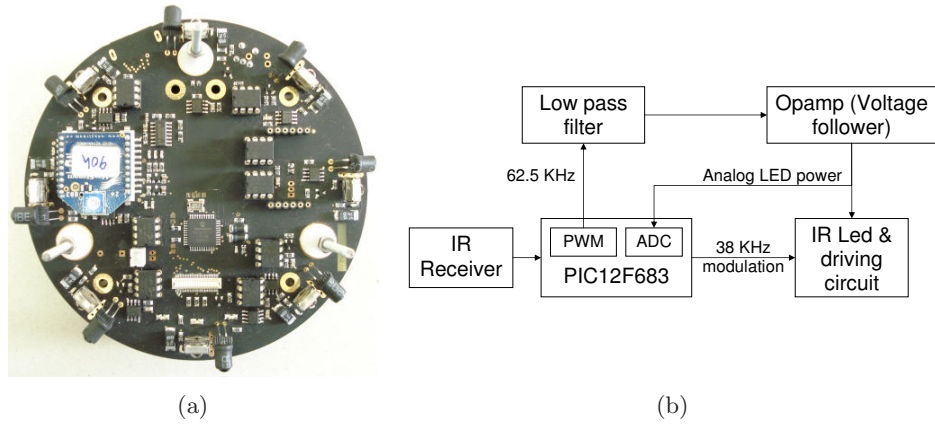


Figure 3.3: (a) Photo of a sensor board. (b) Block diagram of an individual sensor. (Images are taken from [2].)

Figure 3.3(b) illustrates the block diagram of an individual sensor. Each sensor contains an IR LED, an IR receiver, a PIC12F683 microcontroller, a low pass filter, an op-amp and a driving circuit. The function of each component is as follows. The PIC12F683 is responsible for the operation of the sensor and as well as for the transmission of the result to the main sensor controller, the PIC16F877A, upon its request. The pulse width modulation (PWM) module of the PIC12F683, the low-pass filter and the op-amp generate the voltage that drives the IR LED through the driving circuit. There are seven different levels of the voltage used in the measurements. *Level 1* and *Level 7* indicates the minimum and maximum levels of the voltage, respectively. The analog-to-digital converter (ADC) module of the PIC12F683 is used to control whether the desired value of the voltage is reached or not after outputting necessary PWM signals. When the desired voltage level is reached, IR LED is turned on and off at 38 kHz by PIC12F683 and an IR burst is emitted. IR receiver detects IR signals and indicates the detection to the PIC12F683.

The sensing algorithm is given in Algorithm 1. The algorithm iterates on three states transitions between which are controlled by the main sensor microcontroller:

- *Kin-detection*. This is the initial state of the sensor. In this state, the sensor turns off the IR LED and only “listens” to the environment to detect any IR signal. The detection indicates a nearby kin-robot.
- *Proximity-sensing*. In this state, the proximity measurement is performed. Since there can be another sensors around emitting IR signals which would disturb

the measurement, the sensor first checks the environment if there is an incoming IR signal. If an incoming IR signal is detected, the sensor waits for the other sensor to finish its measurement. This is done by looking for a safety interval which takes approximately 6.7 ms without detecting any IR signal. The amount of the interval is the maximum possible time spent by a sensor to detect an object. Here, we should note that the incoming IR signal that causes a delay in the measurement of the sensor could be emitted from a sensor on the same robot, hence can not be inferred as a kin-robot. Upon catching a safety interval, the sensor starts its measurement safely. In the measurement, the sensor determines the minimum voltage level at which an object is detected. This minimum voltage level gives the distance from the object whose kind is determined in the last *kin-detection* state as a kin-robot or an obstacle. For a particular voltage level, object detection is done by first adjusting the voltage to the desired level and then sending an IR burst. The detection of reflecting IR burst by the IR receiver indicates the detection of the object at the corresponding level (See Algorithm 2). In order to determine the distance of an object in a fast way, the sensing algorithm applies a divide and conquer like approach in switching between voltage levels. The algorithm first looks for an object at the minimum voltage level to determine a nearby object in the first place. If an object is not detected at the minimum level, the sensor switches to the maximum level. The detection of an object at the maximum level makes the algorithm to switch to internal levels, whereas, if an object is not detected, it is taken as no detection case. Between the internal levels, the sensor first switches to the middle voltage level (*Level 4*). If an object is detected at the middle level, the sensor switches to lower levels; if not, it switches to upper levels to determine the distance of the object. With this approach, the sensor determines a nearby object and no detection case in a fast way and the distance of an object is measured after at most 5 voltage level switches.

- *Data-transmission.* In this state, the result of the measurement is sent to the main sensor controller. The result of k^{th} sensor is an integer pair (r_k, o_k) . $r_k \in \{0, 1\}$ shows whether the detected object is a kin-robot or not. $o_k \in \{0, 1, \dots, 7\}$ denotes the distance from the object being sensed. $o_k = 1$ and $o_k = 7$ indicate

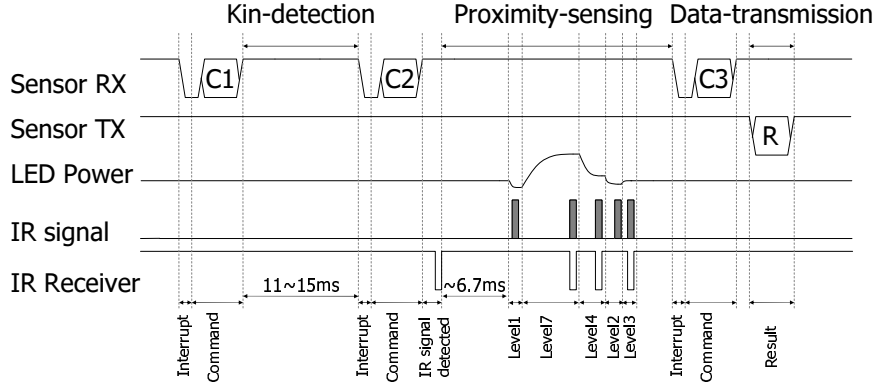


Figure 3.4: Timing diagram of a sensor detecting an obstacle. (Image is taken from [2].)

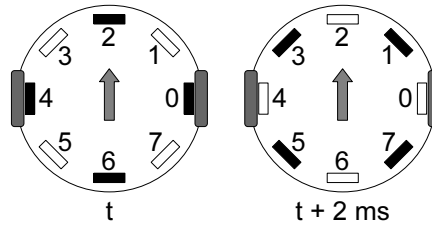


Figure 3.5: The order and timing of sensors put into the *proximity-sensing* state by the main sensor controller. First, even numbered sensors and after 2 ms, odd numbered sensors are put into the *proximity-sensing* state.

a distant and a nearby object, respectively. $o_k = 0$ stands for no detection.

Figure 3.4, depicts the timing diagram of a sensor for detection of an obstacle at *Level 3*. *C1* command puts the sensor in the *kin-detection* state where no IR signal is detected meaning that there is no kin-robot around. Then, after receiving *C2* command, the sensor enters the *proximity-sensing* state. In this state the sensor detects an IR signal and delays its measurement. After the time interval exceeds approximately 6.7 ms without receiving an IR signal, the sensor starts the measurement and detects an obstacle at *Level 3*. The sensor sends the result to the main sensor controller upon receiving the *C3* command.

The main sensor controller is responsible for the coordination of the sensors and the transmission of all results obtained from the sensors to the main processor of the robot. It coordinates the sensors first putting all of them into the *kin-detection* state. The amount of this state is determined randomly between 11-15 ms to guarantee that the sensors of two different robots do not synchronize. After the *kin-detection* state,

Algorithm 1: Sensing algorithm

```
switch STATE do
  /* STATE is set by interrupt service routine (ISR) that
     handles the main sensor controller commands. */
  case Kin-detection
     $r_k=0$ ;
    while STATE = Kin-detection do
      if IR Receiver detected an IR signal then
         $r_k=1$ ;
  case Proximity-sensing
    if measurementCompleted = 0 then
      /* measurementCompleted is cleared in ISR */
      while STATE = Proximity-sensing do
        if IR Receiver detected an IR signal then
          Time = 0;
        else
          Time ++;
          if Time > 6.7 ms then break;
        if lookForObject (Level 1) = 1 then  $o_k=7$ ;
        else if lookForObject (Level 7) = 0 then  $o_k=0$ ;
        else if lookForObject (Level 4) = 1 then
          if lookForObject (Level 2) = 1 then  $o_k=6$ ;
          else if lookForObject (Level 3) = 1 then  $o_k=5$ ;
          else  $o_k=4$ ;
        else
          if lookForObject (Level 5) = 1 then  $o_k=3$ ;
          else if lookForObject (Level 6) = 1 then  $o_k=2$ ;
          else  $o_k=1$ ;
        measurementCompleted = 1;
      break;
  case Data-transmission
    transmit  $r_k$ ;
    transmit  $o_k$ ;
```

Algorithm 2: lookForObject routine

input : An integer, l indicating the voltage level

output: 1, If an object is detected; 0, if not.

Set PWM signal for voltage level l ;

repeat

| Read ADC value.

until $ADC\ value = Desired\ voltage\ level$;

Send an IR burst;

if *IR Receiver detected an IR signal* **then**

| **return** 1;

else

| **return** 0;

the main sensor controller first puts the even numbered sensors into the *proximity-sensing* state as depicted in Figure 3.5. Then, after 2 ms the odd numbered sensors are put into the *proximity-sensing* state. This ensures that two neighboring sensors do not start the measurement at the same time and any interference caused by crosstalk is prevented. After 33 ms which is an appropriate period of time for the sensors to finish their measurements, the sensors are put into the *data-transmission* state and the results are collected. The main sensor controller transmits these results to the main processor via I²C protocol, when requested.

3.1.2 The Heading Sensing Sub-system

The compass and the communication module of the robots are used to create a heading sensing system, called as the *virtual heading sensor* (VHS), which lets the robots to sense the relative headings of their neighbors. At each control step which is approximately 110 ms, a robot measures its own heading (θ) and then broadcasts it to the robots within the communication range. The heading measurement is done in clockwise direction with respect to the *sensed North* as shown in 4.2. The neighbors whose heading values are received in a control step are called as VHS neighbors.

The received heading value (θ_{rj}) from the j^{th} VHS neighbor is converted to the body-fixed reference frame of the robot as¹:

¹ The heading of the robot, θ is the angle between the *sensed North* and the y -axis of its body-fixed reference frame in clockwise direction, see Figure 4.2. $\frac{\pi}{2}$ is added to $\theta - \theta_{rj}$ to obtain the heading of

$$\theta_j = \theta - \theta_{rj} + \frac{\pi}{2} \quad (3.1)$$

where θ_j is the heading of the j^{th} VHS neighbor with respect to the body-fixed reference frame of the robot.

The most important drawback with the VHS is that the hard-iron effect, local changes in the magnetic field of the Earth due to a magnetized ferrous metal or a permanent magnet, causes deviations in the sensed North direction especially indoor environments where the metal objects are abundant.

3.2 The Simulator: Co-Swarm

A physics-based simulator, called Co-Swarm Simulator (CoSS) is used in computer simulations. CoSS is implemented using Open Dynamics Engine (ODE). The body and the wheels of the robot as cylinders and collision of the bodies and slippage in wheels are simulated within ODE.

The actuation and sensing characteristics of the Kobot robot platform are obtained from systematic experiments and implemented in CoSS. IRSS is modelled based on samples collected in real robot experiments performed to characterize the proximal sensing and kin-detection capabilities of the robot [1]. VHS is modelled using the experiments conducted in Prowler [23], an event-driven probabilistic wireless network simulator, to characterize the effect of the wireless communication range (R) to the number of VHS neighbors (N_c) [1]. The range of wireless communication in CoSS is taken as 20 m in accordance with the range of communication module of Kobot. The number of VHS neighbors is limited at 20, a value determined from the experiments performed with Prowler. In a previous study [1], it was shown that results obtained from CoSS were similar to the ones obtained from Kobots.

the j^{th} neighbor in the body-fixed reference frame.

CHAPTER 4

THE FLOCKING BEHAVIOR

In this study, we extend the flocking behavior proposed in [1] to include a homing direction. Specifically, the behavior consists of heading alignment, proximal control and homing components combined in a weighted vector sum:

$$\vec{a} = \frac{\vec{h} + \beta \vec{p} + \gamma \vec{g}}{\|\vec{h} + \beta \vec{p} + \gamma \vec{g}\|} \quad (4.1)$$

where \vec{h} is the heading alignment vector, \vec{p} and \vec{g} are the proximal control and homing direction alignment vectors with weights β and γ respectively. \vec{a} is the desired heading vector for the robot that is normalized by Euclidean norm shown as $\|\cdot\|$.

4.1 Heading Alignment Behavior

The aim of the heading alignment behavior is to align the robot with the average heading of its neighbors. Using the the received headings of the VHS neighbors, the heading alignment vector (\vec{h}) is calculated as:

$$\vec{h} = \frac{\sum_{j \in \mathcal{N}_R} e^{i\theta_j}}{\|\sum_{j \in \mathcal{N}_R} e^{i\theta_j}\|}$$

where \mathcal{N}_R denotes the set of VHS neighbors, when the communication range of VHS is set to R . θ_j is the heading of the j^{th} neighbor in the body-fixed reference frame.

4.2 Proximal Control Behavior

The proximal control behavior aims to maintain the cohesion of the flock while avoiding the obstacles. Using the data obtained from the IRSS, the normalized proximal control vector, \vec{p} , is calculated as:

$$\vec{p} = \frac{1}{8} \sum_{k=1}^8 f_k e^{i\phi_k} \quad (4.2)$$

where k refers to the sensor placed at angle $\phi_k = \frac{\pi}{4}k$ with the x -axis of the body-fixed reference frame (Figure 3.1(b)). f_k is the virtual force applied by the k^{th} sensor to the robot which is calculated as:

$$f_k = \begin{cases} -\frac{(o_k - o_{des})^2}{C} & \text{if } o_k \geq o_{des} \\ \frac{(o_k - o_{des})^2}{C} & \text{otherwise} \end{cases} \quad (4.3)$$

where C is a scaling constant. o_k indicates the detection level for the k^{th} sensor, namely the distance from the object. o_{des} is the desired detection level that is taken as a finite value for kin-robots, and 0 for obstacles. In Figure 4.1, the virtual force is drawn for both obstacles and kin-robots. o_{des} values are also indicated.

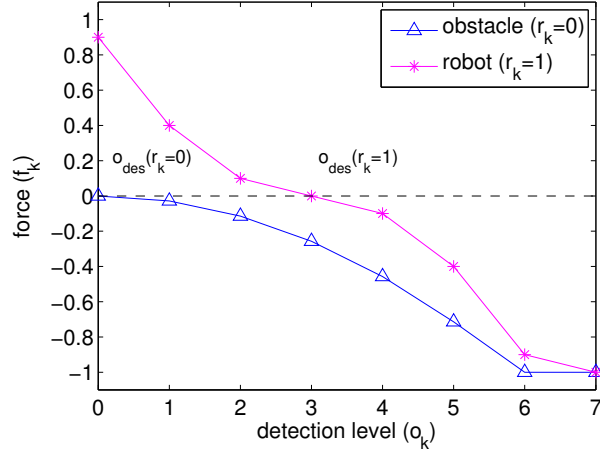


Figure 4.1: Plot of the virtual force with respect to o_k . o_{des} is set to 3 for kin-robots. The value of o_k increases as the distance gets closer. The virtual force always takes values within $[-1, 1]$ interval. (Image is taken from [2].)

4.3 Homing Behavior

The homing behavior aims to align the robot with the desired homing direction (θ_d).

The homing direction alignment vector \vec{g} is calculated as:

$$\vec{g} = \vec{g}_d - \vec{a}_c$$

where \vec{g}_d is the desired homing direction vector in the body-fixed coordinate frame

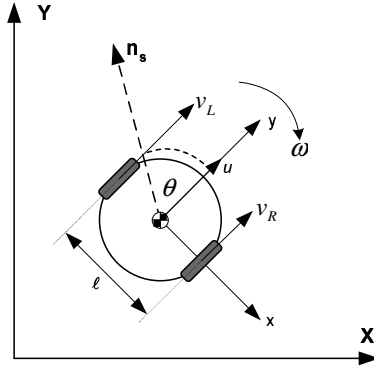


Figure 4.2: The body-fixed reference frame of Kobot is depicted. It is fixed to the center of the robot. The x -axis of the body-fixed reference frame coincides with the rotation axis of the wheels. The forward velocity (u) is along with the y -axis of the body-fixed reference frame. The angular velocity of the robot is denoted with ω . v_R and v_L are the velocities of the right and left motors, respectively. θ , current heading or the robot, is the angle between the y -axis of the body-fixed reference frame and the *sensed North* direction (n_s). l is the distance between the wheels. (Image is taken from [2].)

and \vec{a}_c is the current heading vector of the robot coincident with the y -axis of the body-fixed reference frame (see Figure 4.2).

In this thesis, we assume that the desired homing direction is a constant that is provided to all the robots a priori. The starting point of the flock is fixed and initially all robots are aligned to homing direction. The duration of the travel is predetermined and no landmarks are used. With these assumptions, the behavior can be said to “migrate” a flock of robots to a particular “breeding location” and is only a partial model of long-range animal migration. Since landmarks are used and the goal direction may change during the travel in animal migration, our behavior should be considered to model a part of animal migration in which a long distance is travelled while the goal direction is fixed.

It should be noted that the homing behavior only modulates the orientation of the robot and does not provide a criteria as to whether a homing position is reached or not.

We should also note that the original flocking behavior (corresponding to the case when γ is set to 0) that was proposed in [1], would make the flock to wander aimlessly within an environment, avoiding obstacles on its path, with no preferred direction.

4.4 Motion Control

The forward (u) and angular (ω) velocities are calculated using the desired heading vector (\vec{a}). The forward (u) velocity is calculated as:

$$u = \begin{cases} (\vec{a} \cdot \vec{a}_c) u_{max} & \text{if } \vec{a} \cdot \vec{a}_c \geq 0 \\ 0 & \text{otherwise} \end{cases} \quad (4.4)$$

The dot product of the desired (\vec{a}) and current heading (\vec{a}_c) vectors in Equation 4.4 is used to modulate the forward velocity of the robot. When the robot is moving in the desired direction the dot product results in 1 and the robot attains its maximum forward velocity (u_{max}). If the robot deviates from the desired direction, the dot product and hence u decreases and converges to 0 when the angle between the two vectors gets closer to 90° . If the angle exceeds 90° then the dot product is negative. In this case, u is set to 0 and the robot makes only rotation.

The angular velocity (ω) of the robot is controlled by a proportional controller using the angular difference between the desired and current heading vectors:

$$\omega = (\angle \vec{a}_c - \angle \vec{a}) K_p$$

where K_p is the proportional gain of the controller.

The rotational speeds of the right and left motors (Figure 4.2) are eventually calculated as follows:

$$N_R = \left(u - \frac{\omega}{2}l\right) \frac{60}{2\pi r}$$

$$N_L = \left(u + \frac{\omega}{2}l\right) \frac{60}{2\pi r}$$

where N_R and N_L are the rotational speeds (rotations per minute) of the right and left motors respectively, l is the distance between the wheels of the robot (meters), u is the forward velocity (meters per second) and ω is the angular velocity (radians per second).

CHAPTER 5

EXPERIMENTAL FRAMEWORK

This chapter describes the experimental setups and the metrics utilized to evaluate the accuracy and efficiency of the flocks in long-range migration.

5.1 Setup

The flocking behavior, described in the previous chapter, has a number of parameters; namely the weight of proximal control (β), the weight of goal direction (γ), the proportional gain for angular velocity (K_p), the maximum forward speed (u_{max}) and the desired detection level (o_{des}). The optimization of these parameters is a challenging problem with which we do not deal in the scope of this thesis. Rather, we used a default set of parameters whose sensitivity analysis is performed in [1] and that are known to generate an acceptable flocking behavior in Kobots and in CoSS. These parameters are listed in Table 5.1.

The experiments are conducted in an open and obstacle-free environment with approximately constant magnetic field. Initially the robots are placed on a hexagonal grid with default 25 cm center spacing and aligned to the desired homing direction which is fixed to an a priori determined value for all robots. Figure 5.1 illustrates the placement of the robots for different flock sizes. However, when we need to disable proximal control behavior in our experiments, we increased the spacing to 20 m to hypothetically disable proximal control behavior. In this case, the range of wireless communication is also increased to 1600 m with the same scale up as in inter-robot spacing. The center of flocks is always fixed at the same initial point.

The features specific to the experimental setups of Kobots and CoSS are described below.

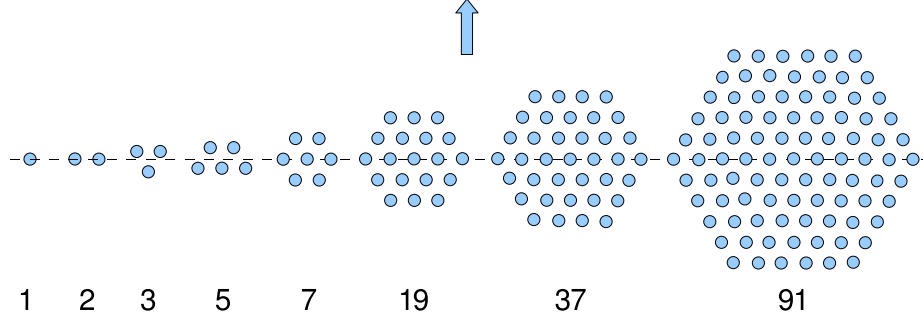


Figure 5.1: The topology of the robots for different flock sizes. The arrow indicates the homing direction.

Table 5.1: The default parameter settings for the behavior.

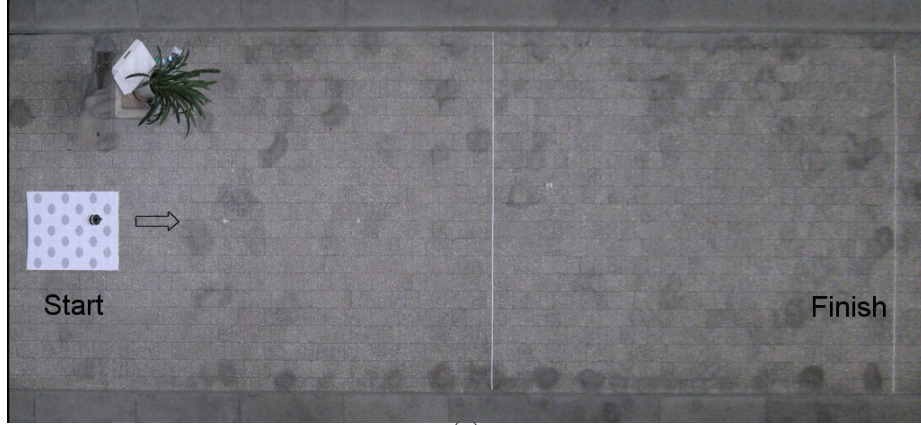
Parameter	Default Value
weight of proximal control (β)	12
weight of goal direction (γ)	4
proportional gain for angular velocity (K_p)	0.5
maximum forward speed (u_{max})	0.07 m/s
desired detection level (o_{des})	3

5.1.1 Kobots

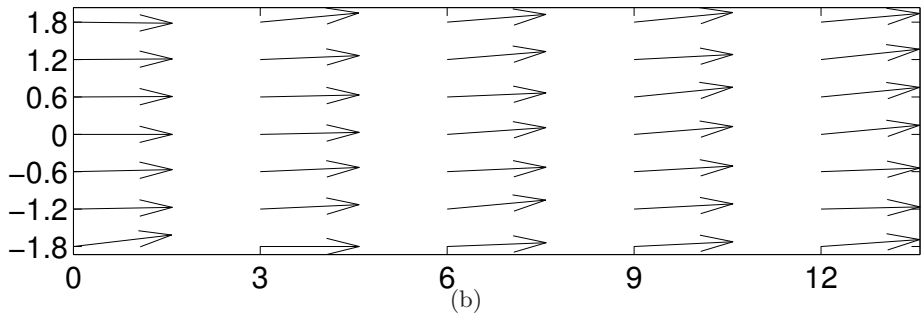
In the experiments conducted with Kobots, we used flocks including up to 7 Kobots. We conducted our experiments in the hall at the deanery building of Faculty of Arts and Sciences at Middle East Technical University, Ankara, Turkey. The arena is of size 4×12 m and is shown in Figure 5.2(a).

The magnetic field in the experiment arena, as shown in Figure 5.2(b), shows that the magnetic field in the arena is not uniform and deviates approximately 6-degrees to the left, between the starting and finishing lines of the course.

The finishing line of the experiment arena at 12 m is marked at equal intervals. At the end of each experiment, a top view image of each robot in the flock is taken with an overhead camera preserving that at least two markers are also included in the image. Using these images, we determine the deviation of the center of each robot from initial direction which is the perpendicular distance of robot center to initial direction. This procedure requires the manual indication of robot center and two markers. Then the deviation of the flock from initial direction is calculated by averaging the deviations



(a)



(b)

Figure 5.2: (a) An overhead view of the experiment arena. (b) The magnetic field measured in the experiment arena. The field is tilted to the left approximately 6-degrees. The units of the axes are in meters.

of the robots in the corresponding flock.

5.1.2 CoSS

In CoSS, the experiments are conducted with flocks that include up to 91 simulated robots. The experiments are executed for 1558 control steps which corresponds to approximately 171.38 seconds of simulated time. This duration is determined from a reference experiment in which a flock of 7 simulated robots traversed 12 m in an ideal world. The length of the experiments can be seen as contradicting with “long-range” term. But, this length is only determined for analysis purposes considering the accordance with real world experiments and the computational costs. The behavior is itself able to migrate the robot flocks to long ranges with the assumptions stated in Section 4.3. In Figure 5.3(a), there is a snapshot of the simulator showing the path followed by a single robot in a world with noise. The uniform magnetic field in the simulator is illustrated in Figure 5.3(b).

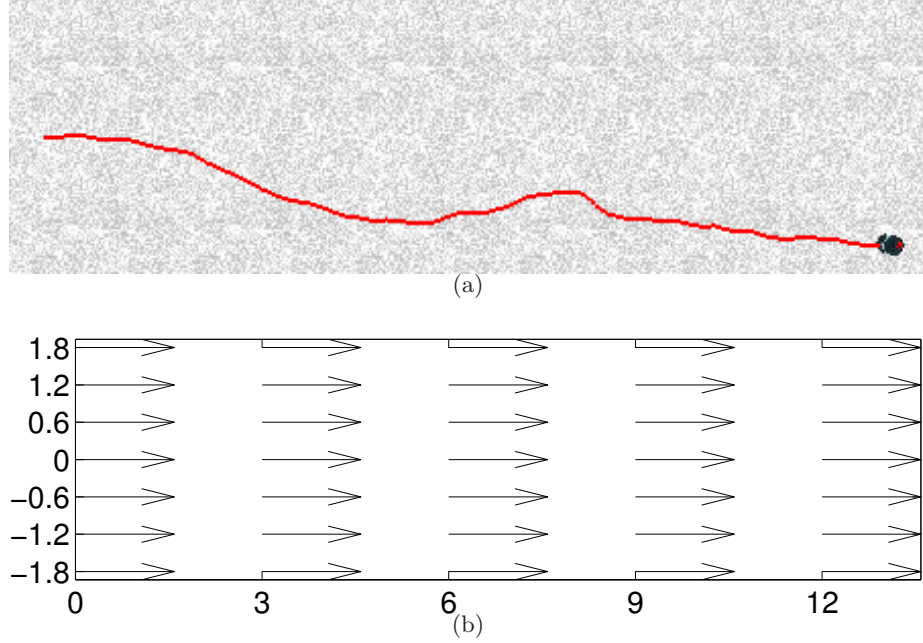


Figure 5.3: (a) The path followed by the center of a single robot. (b) The magnetic field model in the simulations. The units of the axes are in meters.

5.2 Metrics

In this section, we describe two metrics used to evaluate the accuracy and efficiency of the flocks in long-range migration. The first metric includes the inter-quartile and whisker ranges and is used to evaluate the accuracy of flocks in migrating along homing direction. The second metric is defined as the average speed for evaluating the efficiency of movement of flocks.

5.2.1 Inter-quartile and Whisker Ranges

In an ideal world free of noise and other external disturbances, the robots starting from a fixed place would always reach the exact same “breeding ground” at all times with perfect accuracy (Figure 5.4(a)). However in physical systems (whether they are robots or biological organisms), factors such as sensor noise would cause deviations at final positions reached at the end of the migration and hence the accuracy decreases. Therefore, accuracy of a flock in migrating along a homing direction is directly related to the amount of scatter of the paths followed by the flock in different runs.

In order to measure the amount of scatter of the paths, we utilize some parameters obtained from a boxplot plotted using the deviations of the center of the group from

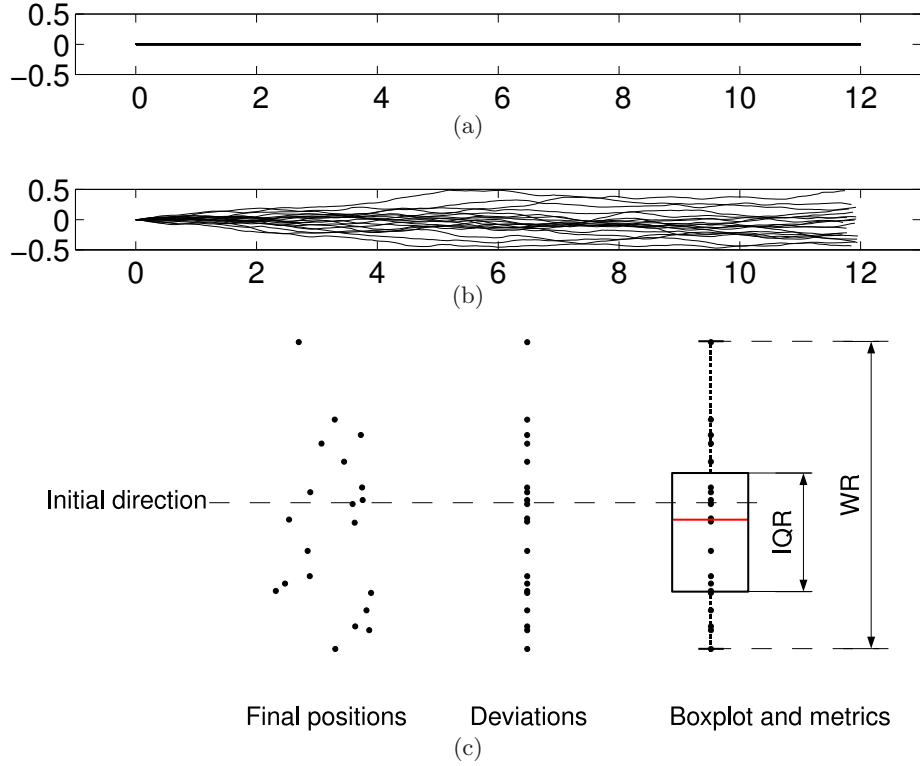


Figure 5.4: (a) In an ideal world, the robots migrate with perfect accuracy. The units of the axes [in (a) and (b)] are in meters. (b) The paths followed by the center of a flock in an environment with noise are drawn for illustrative purposes. (c) Distributions of the center positions, the boxplot of distribution and IQR and WR are illustrated.

initial direction calculated at the final position. The final position is the position reached around the finishing line for Kobots and the position reached at the end of the experiment in CoSS. For example in Figure 5.4(c), the final positions are depicted for the paths given in Figure 5.4(b). The distribution of deviations from initial direction at the final positions are shown in Figure 5.4(c). The boxplot of the distribution of these deviations is plotted on the right side of Figure 5.4(c). In this boxplot, the ends of the boxes and the horizontal line in between correspond to the first and third quartiles and the median values, respectively. The top and bottom whiskers indicate the largest and smallest non-outlier data, respectively. The data in between the first and third quartiles lie within the 50% confidence interval, while the data in between the whiskers lie within the 99.3% confidence interval. The distance between first and third quartiles is called as inter-quartile range (IQR) and the distance between the whiskers is referred as whisker range (WR). We use IQR and WR as a metric to quantify the amount of scatter. Lower values of IQR and WR indicate a more accurate path.

Since we are interested in the scatter, the median of the deviations is not informative for us. The variance of the deviations is also not an appropriate metric because of the possible outliers.

5.2.2 Average Speed

We use average speed (V_a) of flocks calculated by dividing total displacement of a flock to the time of operation as a measure of the efficiency of the movement. A high average speed is a sign of efficient movement driving the flock smoothly whereas a low average speed indicates inefficient and jerky motion.

CHAPTER 6

FACTORS THAT INFLUENCE LONG-RANGE MIGRATION OF FLOCKS

In this thesis, we study, from a constructivist view, how flocking affects the variance in the final positions reached. Moving the flock of robots to an arbitrary “breeding location” in space is out of the scope of this work. Rather we are interested in investigating pros and cons of flocking in the accuracy of motion towards the desired breeding location. Considering the flocking behavior we have developed and as well as the robotic platform we use, we hypothesize that four factors influence this variance in accordance with their possible counterparts involved in animal migration:

- Averaging through heading alignment (HA). The heading alignment behavior aims to align the individuals to the average heading of their neighbors. This allows the individuals to suppress the sensor noise in sensing the homing direction improving the accuracy of their alignment. The dynamics captured here can be considered to correspond to the *many wrongs principle*.
- Noise in sensing the homing direction (HD). The homing direction, typically obtained from Earth’s magnetic field, can be considered to have noise. This noise can be caused by the characteristics of the sensor as well as external fluctuations in the magnetic field. In this study, we use the natural or artificially created noise in the compass of our robots to model this.

The noise in sensing the homing direction is inherent in Kobots due to the hard-iron effect and is modelled in CoSS using the vectorial noise model [24] as:

$$\theta_d = \angle \{ e^{i\theta'_d} + \eta_S e^{i\xi_S} \} \quad (6.1)$$

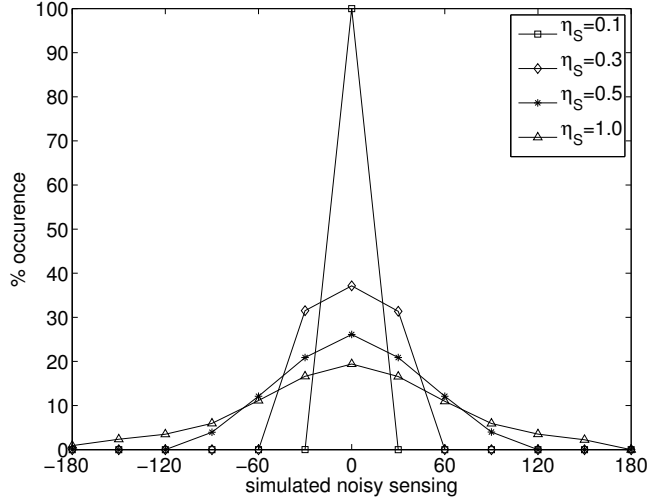


Figure 6.1: Histogram of simulated noisy sensing the homing direction.

where θ'_d represents the actual homing direction, η_S is a parameter determining the magnitude of noise vector and ξ_S is the direction of the noise chosen from a Gaussian distribution $N(\mu = \theta'_d, \sigma = \pm \frac{\pi}{2})$ where μ and σ are the mean and standard deviation, respectively. In the experiments the default value of η_S is taken as 0.5.

We simulated the proposed noise model, in order to demonstrate the nature and the scale of disturbances in the homing directions sensed. Taking θ'_d as 0 and assuming that the noise vector has a distribution characterized by $N(\mu = \theta'_d, \sigma = \pm \frac{\pi}{2})$, we conducted an experiment by varying η_S . We collected 10000 readings for each value of η_S and plotted the histogram of the noisy readings in Figure 6.1. These results show that the standard deviation of the resultant distribution is controlled by the value of η_S .

- Differences in the characteristics of the individuals (CD). Not all individuals in a flock are identical. For example, the birds in a migratory flock have different wing lengths, weights, etcetera. Similarly, even the robots that are manufactured from the same components using the same process, tend to have slightly different sensor/actuator characteristics.

In this study, we assume that the distribution of individual differences at the population level is fixed. Therefore, individuals run without any fail or any other

unexpected behavior during the experiments.

The Kobots are inherently different from each other in terms of actuation as will be investigated later in Chapter 7. In CoSS, we implement the individual differences as a bias term added to the right motor speed as:

$$N_R = N'_R + \xi_m \tag{6.2}$$

where N'_R is the actual speed of the right motor and ξ_m is the bias term in rpm. ξ_m is chosen from a Gaussian distribution $N(\mu = \mu_i, \sigma)$. σ is fixed for all robots as 0.05 rpm, whereas, μ_i for the i_{th} robot is chosen from a Gaussian distribution $N(\mu = 0, \sigma = 0.05)$ to diversify the robots.

This bias gives the robot a tendency to deviate towards to left or right instead of moving straight. The direction of the tendency depends on the sign of μ_i .

- Disturbances caused by proximal control behavior (PD). During flocking, the proximal control behavior aims to keep the flock cohesive yet make sure that no collisions happen among the individuals. This creates disturbances on the heading direction of the individuals.

These disturbances are implicit in the proximal sensing and need not to be explicitly included.

CHAPTER 7

EXPERIMENTS

In the experiments reported in this chapter, we analyze how the four factors described in the previous chapter contribute to the accuracy of long-range migration of robot flocks through experiments conducted with physical and simulated robots.

In an ideal world, where there is no sensing and actuation noise, flocks of all sizes will follow the same straight line as illustrated in Figure 7.1. However, the accuracy of a flock would be affected depending on the parameters under influence of noise, the amount of noise and the size of the flock.

In this chapter, we will add one or more noise sources to the system at a time and then investigate pros and cons of flocking under these disturbing effects to understand whether there is a benefit of flock size or not in terms of accuracy. We conducted four sets of experiments. The factors tested in each set is presented in Table 7.1. Since the heading alignment is crucial for flocking behavior, it is enabled in all experiments without noise.

In the first set of the experiments our aim is to understand the effect of disturbances caused by proximal control. In the second set of the experiments, we evaluate the effect of noise in sensing the homing direction alone. In the third set of the experiments, we added the proximal control behavior while the individuals are identical and the

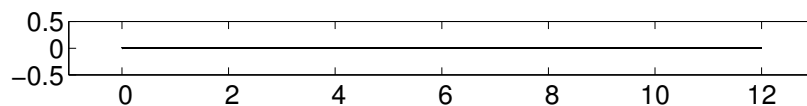


Figure 7.1: With no noise in sensing or actuation the flock of any number of robot always follows the same path. The units of the axes are in meters.

Table 7.1: Investigated factors in the experiments. The four factors considered are HA: Averaging through heading alignment, HD: Noise in sensing the homing direction, CD: Differences in the characteristics of the individuals and PD: Disturbances caused by proximal control behavior.

Experiment	HA	HD	CD	PD	Platform
1	+	-	-	+	CoSS
2	+	+	-	-	CoSS
3	+	+	-	+	CoSS
4a	+	+	+	-	CoSS
4b	+	+	+	+	CoSS & Kobots

noise in sensing the homing direction is also present. The last set of the experiments in which the effect of individual differences is analyzed is divided into two subsets. In the first subset, proximal control is disabled whereas in the second it is enabled.

The first three sets of the experiments and the first subset of the fourth experiment are performed in only simulation while experiment 4b is conducted both in simulations and with Kobots. The experiments performed with CoSS and Kobots are repeated 500 and 5 times, respectively, unless otherwise stated.

7.1 Effect of Proximal Disturbance

The proximal control behavior aims to avoid collisions with robots and obstacles and to maintain the cohesion of the flock using the readings obtained from the IRSS. Since IRSS has a noisy characteristic, the movement of the robots is disturbed due to the false readings. Therefore, the accuracy of the flock in moving along the homing direction is affected.

In order to understand the effect of disturbances caused by the proximal control behavior, we conduct an experiment in which we leave only the IRSS as a source of noise in the system and perform experiments for different flock sizes. In Figure 7.2(a), IQR and WR are plotted for each flock size. Figure 7.2(b) shows the average speeds for different flock sizes.

In Figure 7.2(a), IQR & WR follow a bell-shaped curve trend whose maximum is reached for 3-robot flock. Since the proximal control behavior is implicitly disabled for a “single robot flock”, it follows always the same path resulting a zero IQR & WR.

The average speed of single robot is at its maximum value as expected. For the

increasing flock size the average speed decreases slightly.

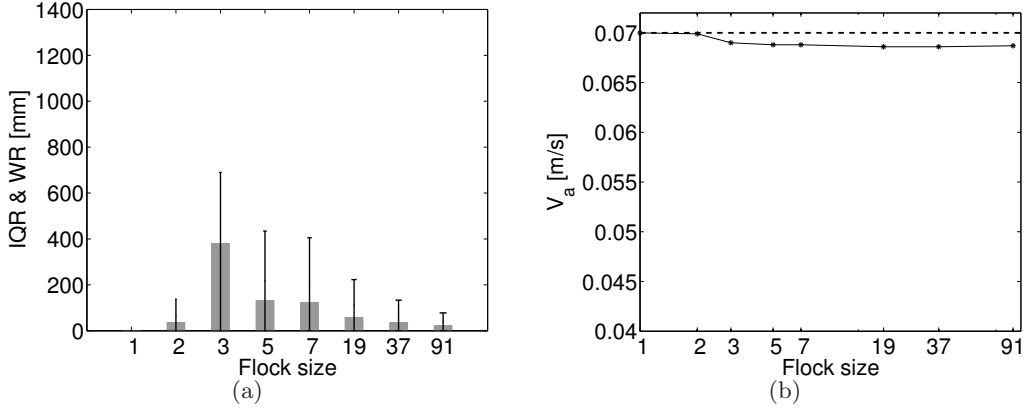


Figure 7.2: (a) Plot of IQR & WR for different flock sizes while the only noise source is proximal control. (b) Plot of average speed for different flock sizes. The horizontal axis is in log scale. The dashed line indicates the value of the maximum forward speed $u_{max} = 0.07$ m/s.

7.2 Effect of Noise in Sensing the Homing Direction

The homing behavior aims to align the robots with the desired homing direction. Therefore, any error in sensing the homing direction would generate undesired deviations in the heading of the robots.

In order to investigate the effect of noise in sensing the homing direction, we varied η_S and conducted experiments with different sizes of flocks composed of identical robots. The proximal control is disabled in the experiments. The paths followed by the flocks for $\eta_S = 0.5$ are plotted in Figure 7.3. Figure 7.4 shows the resulting IQRs of the flocks in different noise conditions. Figure 7.5(a) and 7.5(b) plot the change in IQR & WR for different flock sizes for $\eta_S = 0.1$ and $\eta_S = 0.9$, respectively. In Figure 7.6(a) and 7.6(b), the average speeds are given with respect to flock size and η_S , respectively.

In Figure 7.3, the distribution of the paths gets narrower as the flock size increases. This is an indication of increase in the accuracy of the flocks with the flock size.

In Figure 7.4, we see that the IQR is zero for all flock sizes when $\eta_S = 0$, which corresponds to the ideal case. When we increase the noise, IQR of small flocks increases rapidly while the increase in IQR of large flocks is slow. In a large flock, the individuals have more VHS neighbors with more variety and therefore, the efficiency of

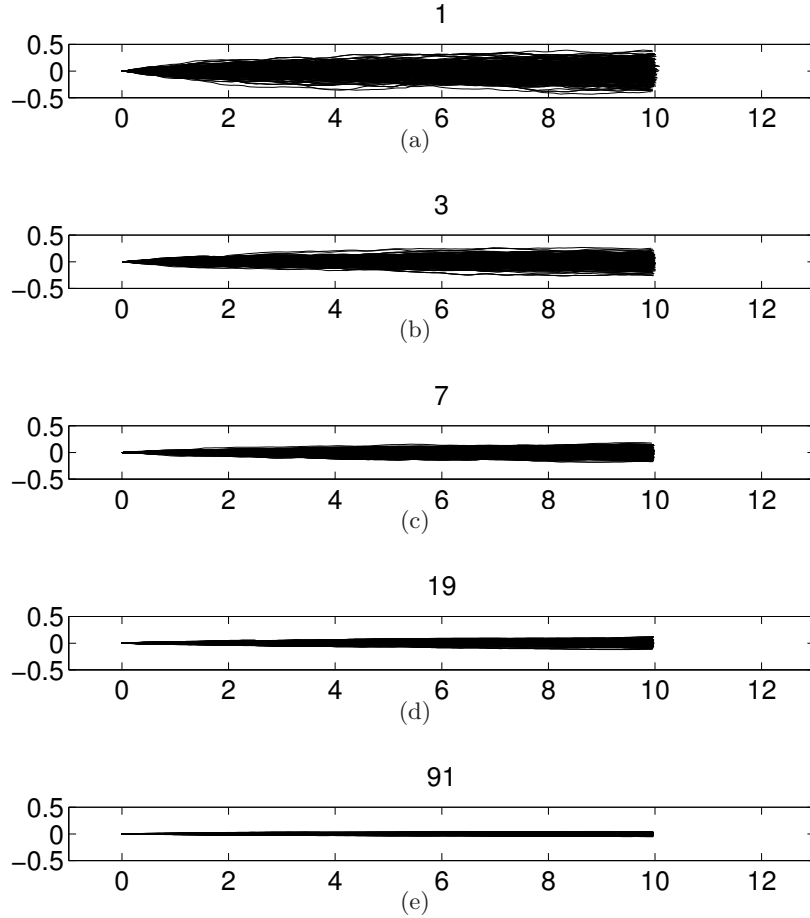


Figure 7.3: The paths followed by the flocks for $\eta_S = 0.5$. The units of the axes are in meters. $[0,0]$ is the starting point. (a) 1 robot, (b) 3 robots, (c) 7 robots, (d) 19 robots, (e) 91 robots.

the averaging through heading alignment increases creating a robustness to the noise.

In Figure 7.5(a) and 7.5(b), both IQR and WR show a decreasing trend as the flock size increases. In both figures, the advantage of large flock size is evident in suppressing the noise in sensing the homing direction more efficiently.

The average speeds in Figure 7.6(a) and 7.6(b) decrease for the increasing noise and remain almost constant for the increasing flock size. The decrease in the average speeds for the increasing noise is a result of large fluctuations in homing direction that cause the robots to turn more and hence get slower. For a fixed η_S , one may expect that as the flock gets larger, the number and variety of VHS neighbors interacted would increase and the fluctuations in the homing direction would be suppressed more efficiently. This would eventually results in an increase in the average speeds of large

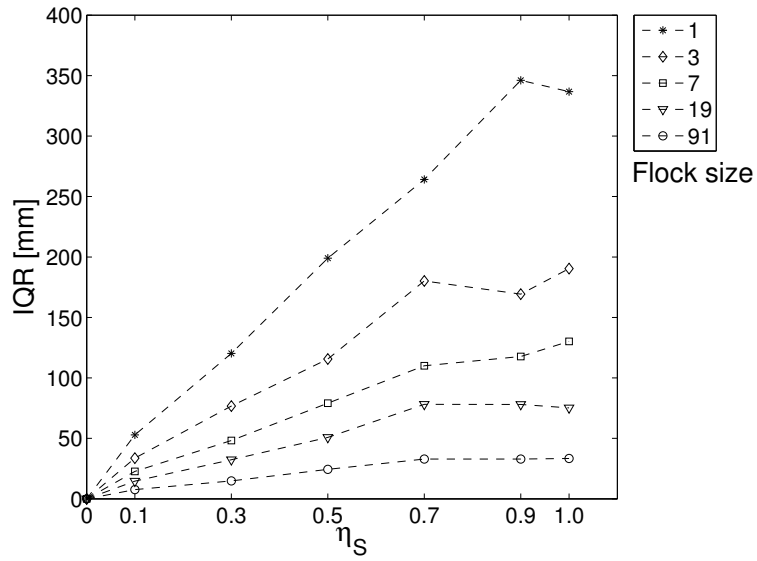


Figure 7.4: Effect of η_S . Plot of IQR with respect to η_S for different flock sizes.

flocks. However, our results are insufficient to explain why the average speeds remain almost constant as the flock size increases and it needs further investigation.

7.3 Effect of Proximal Disturbance with Noise in Sensing the Homing Direction

We repeated the second set of the experiments with the proximal control behavior is enabled. The noise in sensing the homing direction is also included in order to understand the combined effect of both factors.

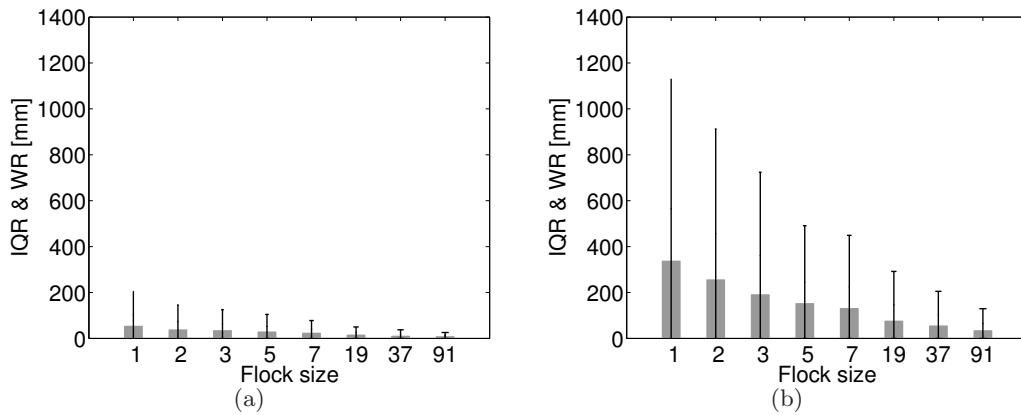


Figure 7.5: Plot of IQR & WR for different flock sizes while (a) $\eta_S = 0.1$, (b) $\eta_S = 0.9$.

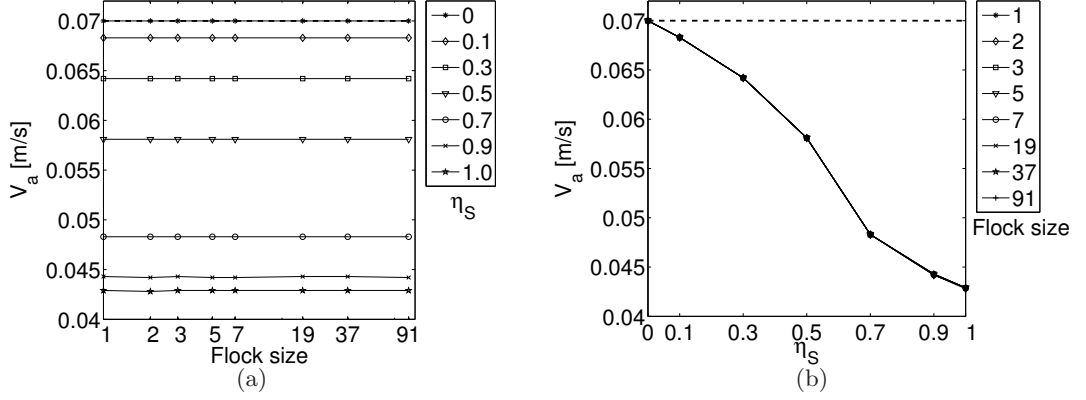


Figure 7.6: (a) Plot of V_a with respect to flock size for different values of η_S . Horizontal axis is in log scale. (b) Plot of V_a with respect to η_S for different flock sizes. The dashed lines indicate the value of the maximum forward speed $u_{max} = 0.07$ m/s.

Plot of IQRs with respect to η_S is given in Figure 7.7 for different values of flock size. Figure 7.8(a) and 7.8(b) illustrates the change in IQR & WR for different flock sizes for $\eta_S = 0.1$ and $\eta_S = 0.9$, respectively. The changes in the average speeds with respect to flock size and η_S are plotted in Figure 7.9(a) and 7.9(b), respectively.

In Figure 7.7, IQR of 1-robot flock increases rapidly as η_S gets larger, whereas IQR of 91-robot flock shows only a slight increase. This indicates the remedial effect of large flock size. As the flock size gets larger, robustness to noise increases as a result of large number of varying VHS neighbors utilized in heading alignment behavior. $\eta_S = 0$ in Figure 7.7 corresponds to the first set of the experiments where the only noise source is proximal control. In this case, the peak in the IQR of 3-robot flock is prominent in parallel to the results obtained in the first set of the experiments. However, the increase in the IQR of 3-robot flock due to proximal disturbances is suppressed when the noise is increased. This interesting dynamic could be a result of discrete size effects and needs further investigation.

In Figure 7.8(a), the effect of proximal disturbances is prominent due to the small amount of noise and we have a similar trend as in Figure 7.5(a) which shows the effect of only proximal control. When the noise is increased, the trend changes as shown in Figure 7.8(b). Beginning from a high value, IQR & WR decrease with the flock size.

Average speeds in Figure 7.9(a) and 7.9(b) decrease as the noise gets larger. As the flock size increases, the average speed decreases slightly for small values of η_S . But, the average speed remains almost constant for high values of η_S .

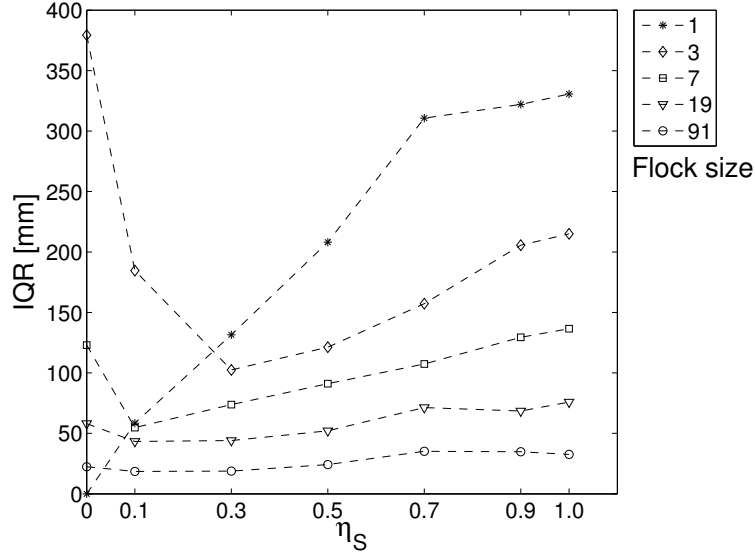


Figure 7.7: Plot of IQR with respect to η_S for different flock sizes.

7.4 Effect of Individual Differences with Noise in Sensing the Homing Direction

If the individuals of a flock have different actuation characteristics, each of them is likely to follow a different path when they “migrate” alone. These different paths of different individuals create a large distribution in total. But what if they are “migrate” together? Could there be an improvement in the accuracy? In the last set of the experiments, we search for answers to these questions.

We split the experiments conducted in this section into two subsets. In the first subset, we conduct experiments only in CoSS and disabled the proximal control by increasing the inter robot distance to 20 m as mentioned in Chapter 5. In the second subset of the experiments, we enabled the proximal control and conducted experiments with CoSS and Kobots. In CoSS experiments, a noise with $\eta_S = 0.5$ is used in sensing the homing direction. In Kobots, this noise is assumed to be inherent due to the hard-iron effect of the metal objects in the environment.

In order to model the individual differences in simulations, we diversify the robots by adding actuation noises as described in Chapter 6. Having diversified 91 robots, we first perform an experiment by running each robot separately. The results are given in Figure 7.10. As can be seen, the differences between the robots are large.

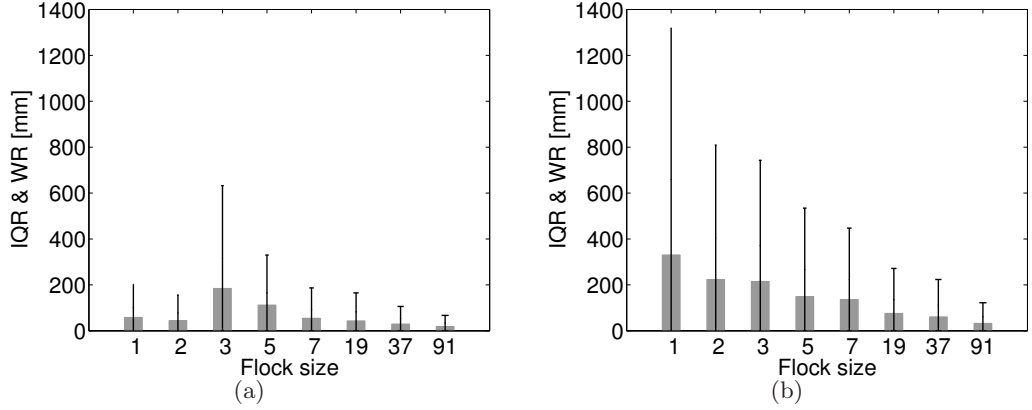


Figure 7.8: Plot of IQR & WR in proximal disturbance experiments for different flock sizes while (a) $\eta_S = 0.1$, (b) $\eta_S = 0.9$.

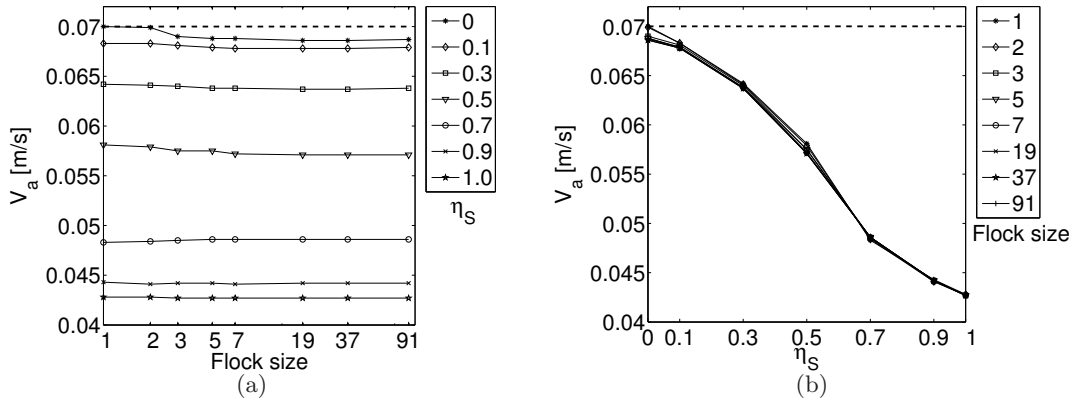


Figure 7.9: (a) Plot of V_a with respect to flock size in proximal disturbance experiments for different values of η_S . Horizontal axis is in log scale. (b) Plot of V_a with respect to η_S for different flock sizes. The dashed lines indicate the value of the maximum forward speed $u_{max} = 0.07$ m/s.

Then, we create flocks of different sizes from the 91 diversified robots to be used in the CoSS experiments. The selection is done in a random fashion and Table 7.2 shows the number of different flocks for each size. The number of different flocks are kept constant for different sizes to guarantee that the IQR and WR metrics are calculated over the same number of experiments. For a flock size of 91, we obtain different flocks by changing the initial positions of the robots.

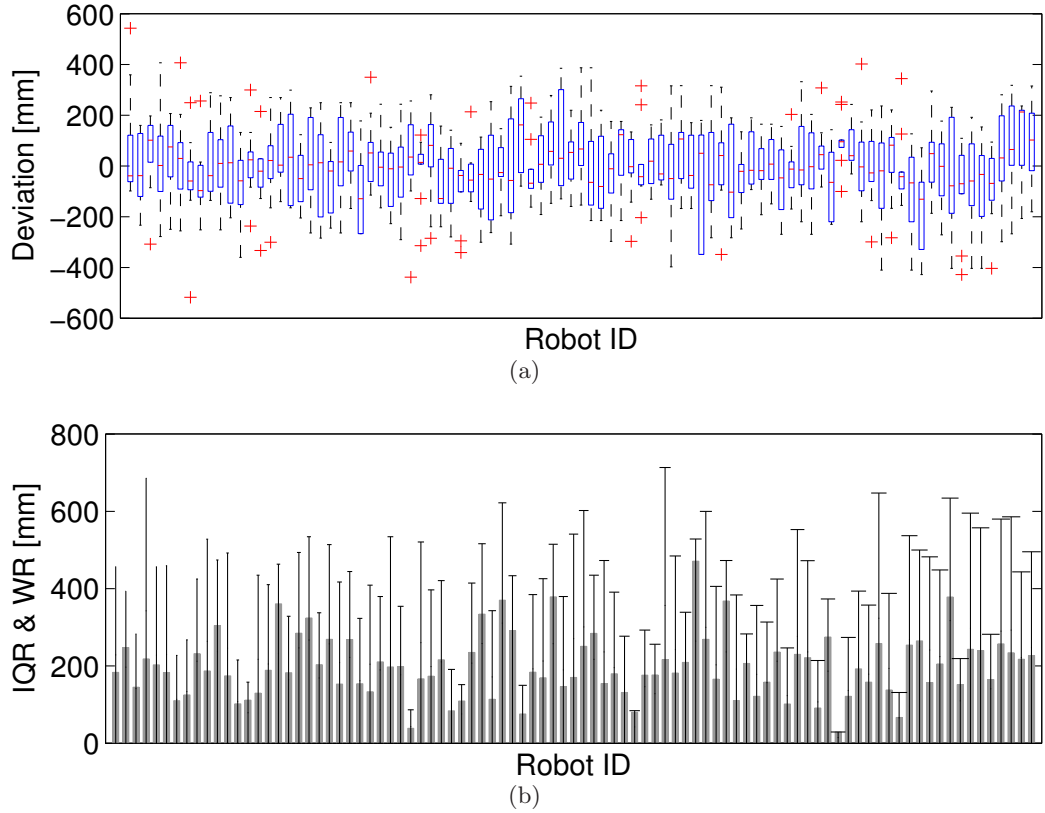


Figure 7.10: Characteristics of different robots after adding actuation noise. (a) Boxplot of deviations, (b) IQR & WR plots.

Table 7.2: The number of the groups selected from 91 diversified robots randomly.

Flock size	1	2	3	5	7	19	37	91
# of different flocks	91	91	91	91	91	91	91	91

7.4.1 Without Proximal Control

By using different flocks constituted from 91 diversified robots, we performed experiments by disabling the proximal control behavior and repeating the experiments 10 times for each flock. From these experiments, the IQR & WR are plotted for different flock sizes in Figure 7.11. In Figure 7.11, the metrics for a particular flock size are calculated using the combined distribution of all different flocks. As can be seen, the IQR & WR decreases indicating the increase in the accuracy while the flock size increases. This clearly shows that the tendencies of the individuals to migrate to different directions are suppressed with heading alignment and the effect of the suppression increases

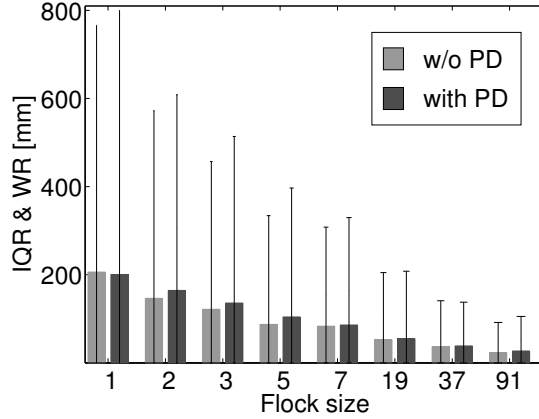


Figure 7.11: IQR & WR plots for individual difference experiments while the proximal control is disabled and enabled.

as the flock size gets larger resulting in an increase in the accuracy.

7.4.2 With Proximal Control

The experiments in this subset are performed in COSS and with physical robots while the proximal control is enabled.

7.4.2.1 CoSS Experiments

In this experiment, we enabled the proximal control behavior and performed the same experiments performed in Section 7.4.1 and plotted the resulting IQR & WR again in Figure 7.11. As can be seen the IQR & WR decreases while the flock size increases, which is an indication of improvement in the accuracy through the suppression of tendencies of the individuals to migrate to different directions via heading alignment. The IQR & WR values are a little bit higher than the experiments without proximal control due to the effect of disturbances of proximal control.

7.4.2.2 Kobot Experiments

The Kobots are inherently not identical. The inequalities in the sensing system are quite acceptable due to the precise manufacturing processes. However, this is not the case for the actuation system.

Therefore we evaluated the actuation characteristics of each robot we use. In this experiment, we do not utilize the flocking behavior. Instead, we commanded the

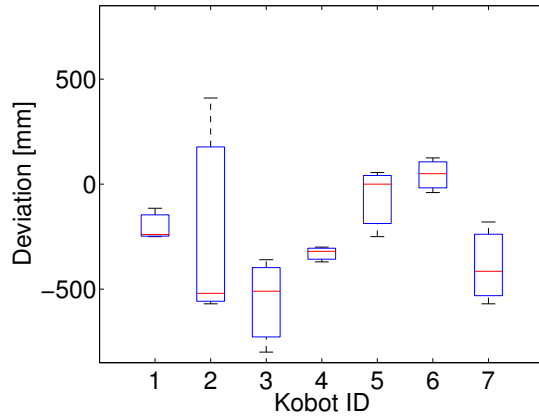


Figure 7.12: Actuation characteristics of Kobots at 2 m while moving forward.

robots to move forward and measured the deviation of the robots from initial direction in each run at 2 m. Figure 7.12 shows the distribution of the deviations for each robot for 3 different runs. As can be seen, the characteristics of the robots differ much from each other. The main reason of these large differences is the lack of a closed-loop speed control for the DC motors of the robots.

In order to understand the effect of group size in real-world conditions, we first conducted experiments with single robots. The resulting distributions of deviations at final position and IQR and WR metrics are given in Figure 7.13(a) and Figure 7.13(b), respectively. Then, we perform experiments with 1-, 3-, 5- and 7-Kobot flocks by selecting 7 different flocks for each flock size. Figure 7.14 illustrates the selection and initial placement of the flocks. Performing only one experiment for a particular flock in Figure 7.14, we plotted IQR and WR for each flock size in Figure 7.15. IQR and WR values for a particular flock size in Figure 7.15 are calculated using the combined distribution of 7 experiments performed for that flock size. Other than 3-Kobot flocks, there is a decreasing trend in IQR and WR indicating that the increase in the flock size increases the accuracy which is similar to the results obtained in simulations.

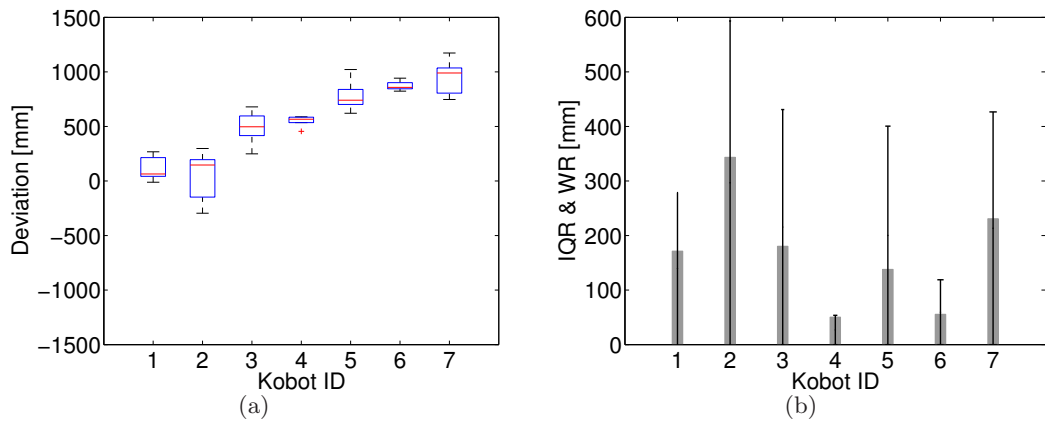


Figure 7.13: The individual differences between Kobots. (a) Distribution of deviations at final position are given. Note that due to a 6-degrees deviation to the one side of the corridor, deviation values are mostly negative. (b) IQR and WR plots calculated from the boxplots in (a).

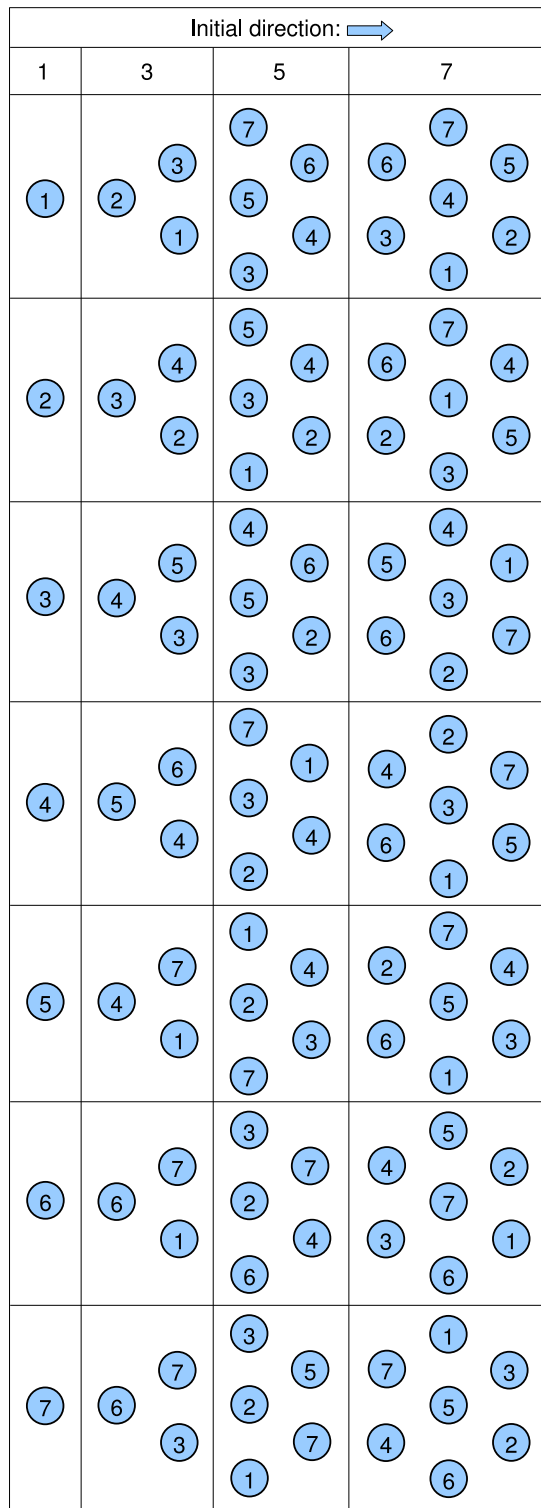


Figure 7.14: The selection and initial placement of the flocks are given for Kobot experiments.

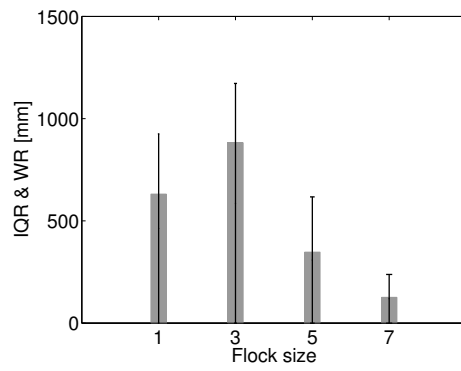


Figure 7.15: IQR and WR of joint distributions of single robot experiments and two 5-Kobot flocks and 7-Kobot flock.

CHAPTER 8

CONCLUSION

This thesis investigated the pros and cons of flocking in long-range migration of mobile robot swarms under influence of different factors. We present a flocking behavior as an extended version of a self-organized flocking behavior based on three simple behaviors: (1) heading alignment, (2) proximal control, and (3) alignment to the desired homing direction. The behavior migrates a flock of robots from one place to another utilizing the magnetic field of the earth. The aim of the behavior is to move the flock to a “breeding location” rather than moving to an arbitrary location.

We pointed out four factors that influence the accuracy of the behavior in reaching the desired breeding location. These are: (1) averaging through the heading alignment behavior, (2) the sensor noise in sensing the homing direction, (3) differences in the characteristics of the individuals, and (4) disturbances caused by proximal control behavior. The pros and cons of flocking is investigated under effect of these factors via experiments conducted both physical and simulated robots. We found that:

- The effect of proximal disturbances makes a peak for a 3-robot flock and is then suppressed with the increasing flock size.
- The increase in the sensor noise in sensing the homing direction results in a decrease in the accuracy of flocks. The smaller flocks are affected more than larger flocks.
- When both proximal disturbances and sensor noise affects the behavior, the effect of proximal disturbances, which creates a peak for a 3-robot flock, disappears as the noise increases.
- For a fixed amount of sensor noise, the average speed does not change with the

flock size. But the increase in noise decreases the average speed.

- The disturbances of proximal control behavior decreases the average speed slightly as the flock size increases.
- When the individual characteristics differ from each other, the flocking improves the accuracy of the behavior.

REFERENCES

- [1] A. E. Turgut, H. Çelikkanat, F. Gökçe, and E. Şahin, “Self-organized flocking in mobile robot swarms,” *Swarm Intelligence*, vol. 2, no. 2-3, 2008.
- [2] A. E. Turgut, *Self-Organized Flocking with a Mobile Robot Swarm*. PhD thesis, Middle East Technical University, Ankara, Turkey, 2008.
- [3] E. Şahin, “Swarm robotics: From sources of inspiration to domains of application,” in *Swarm Robotics Workshop: State-of-the-art Survey* (E. Şahin and W. Spears, eds.), no. 3342 in Lecture Notes in Computer Science, (Berlin Heidelberg), pp. 10–20, Springer-Verlag, 2005.
- [4] J. Perrin, “Winged migration.” <http://www.sonyclassics.com/wingedmigration/home.html>, Last visited: September 2008.
- [5] R. C. Beason, “Mechanisms of magnetic orientation in birds,” *Integrative and Comparative Biology*, vol. 45, pp. 565–573, June 2005.
- [6] H. G. Wallraff, *Avian Navigation: Pigeon Homing as a Paradigm*. Berlin: Springer-Verlag, 2005.
- [7] W. Wiltschko and R. Wiltschko, “Magnetic orientation and magnetoreception in birds and other animals,” *Journal of Comparative Physiology A: Neuroethology, Sensory, Neural, and Behavioral Physiology*, vol. 191, pp. 675–693, August 2005.
- [8] D. Heyers, M. Manns, H. Luksch, O. Gunturkun, and H. Mouritsen, “A visual pathway links brain structures active during magnetic compass orientation in migratory birds,” *PLoS ONE*, vol. 2, no. 9, p. e937, 2007.
- [9] S. A. Rommel, Jr., and J. D. McCleave, “Prediction of oceanic electric fields in relation to fish migration,” *ICES Journal of Marine Science*, vol. 35, no. 1, pp. 27–31, 1973.
- [10] S. M. Perez, O. R. Taylor, and R. Jander, “A sun compass in monarch butterflies,” *Nature*, vol. 387, no. 6628, p. 29, 1997.
- [11] G. Bergman and K. Donner, “An analysis of the spring migration of the common scoter and the long-tailed duck in southern finland,” *Acta Zool. Fenn.*, vol. 105, pp. 1–59, 1964.
- [12] W. Hamilton, “Social aspects of bird orientation mechanisms,” *Animal Orientation and Navigation*, pp. 57–71, 1967.
- [13] H. G. Wallraff, “Social interrelations involved in migratory orientation of birds: Possible contribution of field studies,” *Oikos*, vol. 30, pp. 401–404, 1978.
- [14] J. Rabøl and H. Noer, “Spring migration in the skylark (*alauda arvensis*) in denmark. influence of environmental factors on the flocksize and migratory direction,” *Vogelwarte*, vol. 27, pp. 50–65, 1973.

- [15] S. Tamm, “Bird orientation: Single homing pigeons compared with small flocks,” *Behavioral Ecology and Sociobiology*, vol. 7, pp. 319–322, 1980.
- [16] W. Keeton, “Comparative orientational and homing performances of single pigeons and small flocks,” *Auk*, vol. 87, pp. 797–799, 1970.
- [17] S. Benvenuti and N. Baldaccini, “Pigeon orientation: A comparison between single birds and small flocks,” *Ornis Scandinavica*, vol. 16, pp. 45–48, 1985.
- [18] T. Guilford and J. Chappell, “When pigeons home alone: Does flocking have a navigational function?,” *Biological Sciences*, vol. 263, no. 1367, pp. 153–156, 1996.
- [19] A. M. Simons, “Many wrongs: The advantage of group navigation,” *Trends in Ecology and Evolution*, vol. 19, no. 9, pp. 453–455, 2004.
- [20] P. A. Hancock, E. Milner-Gullanda, and M. J. Keeling, “Modelling the many-wrongs principle: The navigational advantages of aggregation in nomadic foragers,” *Journal of Theoretical Biology*, vol. 240, pp. 302–310, 2006.
- [21] E. Codling, J. Pitchford, and S. Simpson, “Group navigation and the “many-wrongs principle” in models of animal movement,” *Ecology*, vol. 88, no. 7, pp. 1864–1870, 2007.
- [22] A. Gutierrez, A. Campo, F. C. Santos, C. Pinciroli, and M. Dorigo, *Social Odometry in Populations of Autonomous Robots*. Lecture Notes in Computer Science, Springer-Verlag.
- [23] G. Simon, P. Volgyesi, M. Maroti, and A. Ledeczki, “Simulation-based optimization of communication protocols for large-scale wireless sensor networks,” in *Proc. of the IEEE Aerospace Conference*, vol. 3, (Big Sky, MT), pp. 1339–1346, March 2003.
- [24] G. Gregoire and H. C. Y. Tu, “Moving and staying together without a leader,” *Physica D*, no. 181, pp. 157–170, 2003.